DR. SHITOU WU (Orcid ID : 0000-0002-8420-9877)

DR. YUE-HENG YANG (Orcid ID : 0000-0002-2504-1111)

DR. KLAUS PETER JOCHUM (Orcid ID : 0000-0002-0135-4578)

DR. JAN DE HOOG (Orcid ID : 0000-0002-5930-3597)

DR. ZHIAN BAO (Orcid ID : 0000-0002-0637-7170)

MR. GUOQIANG TANG (Orcid ID : 0000-0001-7754-9390)

DR. LIANJUN FENG (Orcid ID : 0000-0002-0325-3789)

DR. HUIMIN YU (Orcid ID : 0000-0001-7299-5009)

MR. LE ZHANG (Orcid ID : 0000-0001-9161-0653)

DR. DING-SHUAI XUE (Orcid ID : 0000-0002-0750-0804)

DR. HAO WANG (Orcid ID : 0000-0002-0021-7563)

DR. MAOYONG HE (Orcid ID : 0000-0002-9545-5037)

DR. CHAOFENG LI (Orcid ID : 0000-0001-8017-5721)

PROF. QIULI LI (Orcid ID : 0000-0002-7280-5508)

DR. XIANHUA LI (Orcid ID : 0000-0001-5512-7736)

Article type : Original Article

Isotopic Compositions (Li-B-Si-O-Mg-Sr-Nd-Hf-Pb) and $Fe^{2+}/\Sigma Fe$ Ratios of Three Synthetic Andesite Glass Reference Materials (ARM-1, ARM-2, ARM-3)

Shitou **Wu** (1, 2)*, Yueheng **Yang** (1, 2), Klaus Peter **Jochum** (3), Rolf L. **Romer** (4), Johannes

Glodny (4), Ivan P. **Savov** (5), Samuele **Agostini** (6), Jan C.M. **De Hoog** (7), Stefan T.M. **Peters** (8), Andreas **Kronz** (8), Chao **Zhang** (9, 10), Zhian **Bao** (9), Xiaojun **Wang** (9), Youlian **Li** (1, 2), Guoqiang **Tang** (1, 2), Lianjun **Feng** (1, 2), Humin **Yu** (11), Zhenxin **Li** (11), Le **Zhang** (12), Jie **Lin** (13), Yuan **Zeng** (14), Chunxue **Xu** (15), Yaping **Wang** (15), Zhu **Cui** (16), Li **Deng** (17), Jun **Xiao** (17), Yanhong **Liu** (1, 2), Dingshuai **Xue** (1, 2), Di **Zhang** (1, 2), Lihui **Jia** (1, 2), Hao **Wang** (1, 2), Lei **Xu** (1, 2), Chao **Huang** (1, 2), Liewen **Xie** (1, 2), Andreas **Pack** (8), Gerhard **Wörner** (8), Maoyong **He** (17), Chaofeng **Li** (1, 2), Honglin **Yuan** (9), Fang **Huang** (11), Qiuli **Li** (1, 2), Jinhui **Yang** (1, 2), Xianhua **Li** (1, 2) and Fuyuan **Wu** (1, 2)

(1) State Key Laboratory of Lithospheric Evolution, Institute of Geology and Geophysics, Chinese Academy of Sciences, Beijing 100029, P.R. China

(2) Innovation Academy for Earth Science, Chinese Academy of Sciences, Beijing, 100029, P.R. China

(3) Department of Climate Geochemistry, Max Planck Institute for Chemistry, P.O.B. 3060, D-55020 Mainz, Germany

(4) Section of Inorganic and Isotope Geochemistry, GFZ German Research Centre for Geosciences, Telegrafenberg, D-14473 Potsdam, Germany

(5) School of Earth and Environment, University of Leeds, Leeds, LS2 9JT, United Kingdom

(6) Istituto di Geoscienze e Georisorse, Consiglio Nazionale delle Ricerche, Pisa, 56124, Italy

(7) School of Geoscience, University of Edinburgh, Edinburgh, EH9 3FE, United Kingdom

(8) Geowissenschaftliches Zentrum, Göttingen Universität, Göttingen 37077, Germany

(9) State Key Laboratory of Continental Dynamics, Department of Geology, Northwest University, Xi'an 710069, P.R. China

(10) Institute of Mineralogy, Leibniz University Hannover, Callinstr. 3, 30167 Hannover, Germany

(11) CAS Key Laboratory of Crust-Mantle Materials and Environments, School of Earth and Space Sciences, University of Science and Technology of China, Hefei, Anhui 230026, P.R. China

(12) State Key Laboratory of Isotope Geochemistry, Guangzhou Institute of Geochemistry, Chinese Academy of Sciences, Guangzhou, Guangdong, 510640, P.R. China

(13) State Key Laboratory of Geological Processes and Mineral Resources, China University of Geosciences, Wuhan, Hubei, 430074, P.R. China

(14) Beijing Research Institute of Uranium Geology, Beijing 100029, P.R. China.

(15) National Research Center for Geoanalysis, Beijing, 100037, P.R. China

(16) China Building Materials Academy, Beijing, 100024, P.R. China

(17) State Key Laboratory of Loess and Quaternary Geology, Center for Excellence in Quaternary Science and Global Change, Institute of Earth Environment, Chinese Academy of Sciences, Xi'an 710061, P.R. China

* Corresponding author. e-mail: shitou.wu@mail.iggcas.ac.cn

Abstract

To expand the newly developed ARM glasses as reference materials for *in situ* microanalysis of isotope ratios and iron oxidation state by a variety of techniques such as SIMS, LA-MC-ICP-MS and EPMA, we report Li-B-Si-O-Mg-Sr-Nd-Hf-Pb isotope data and $Fe^{2+}/\Sigma Fe$ ratios for these glasses. The data were mainly obtained by TIMS, MC-ICP-MS, IR-MS and wet-chemistry colorimetric techniques. The quality of these data was cross-checked by comparing different techniques or by comparing the results from different laboratories using the same technique. All three glasses appear to be homogeneous with respect to the investigated isotope ratios (except for B in ARM-3) and $Fe^{2+}/\Sigma Fe$ ratios at the scale of sampling volume and level of the analytical precision of each technique. The homogeneity of Li-B-O-Nd-Pb isotope ratios at the micro scale (30–120 μm) was estimated using LA-MC-ICP-MS and SIMS techniques. We also present new EPMA major element data obtained using three different instruments for the glasses. The determination of reference values for the major elements and their uncertainties at the 95% confidence level closely followed ISO guidelines and the Certification Protocol of the International Association of Geoanalysts. The ARM glasses may be particularly useful as reference materials for *in situ* isotope ratio analysis.

Keywords: *In situ* isotope ratio analysis, iron oxide state, ARM glasses, reference materials, LA-(MC)-ICP-MS.

Received 24 Sep 20 – Accepted 07 Jun 21

Advances in micro-analytical techniques, such as SIMS, LA-MC-ICP-MS and micro X-ray fluorescence spectrometry (μ-XRF), continue to revolutionise geochemistry. The latest developments in instrumentation and methodology allow the extraction of geochemical and isotopic tracer information at a spatial resolution of < 20 μm (Liu *et al.* 2011, Ibanez-Mejia *et al.* 2014, Sylvester and Jackson 2016, Woodhead *et al.* 2016, Xie *et al.* 2017, Wu *et al.* 2019, Liu *et al.* 2020, Wu *et al.* 2020). Reference glass materials play an important role for *in situ* microanalysis (Jochum and Enzweiler 2014). Such reference materials are commonly used for

calibration, quality control and inter-laboratory comparison of analytical data (Jochum and Enzweiler 2014). Currently, approximately 20 reference glasses are available to the geochemical community. Most of these reference materials have been well characterised for their mass fractions and isotope ratios. These include the synthetic soda-lime glasses NIST SRM 610/612/614/616 (Pearce *et al.* 1997, Rocholl *et al.* 1997, Woodhead and Hergt 2001, Woodhead 2002, Baker *et al.* 2004, Nebel *et al.* 2009, Jochum *et al.* 2011a), MPI-DING glasses (KL2-G, ML3B-G, StHs6/80-G, GOR128-G, GOR132-G, BM90/21-G, ATHO-G and T1-G) (Jochum *et al.* 2000, 2005a, 2006, 2011b), USGS glasses (BCR-2G, BHVO-2GK, BIR-1G and basaltic GS synthetic glasses) (Woodhead and Hergt 2001, Elburg *et al.* 2005, Guillong *et al.* 2005, Jochum *et al.* 2005b) and Chinese Geological Standard Glass (CGSG-1, -2, -4 and -5) (Hu *et al.* 2011, Denton *et al.* 2013, Yang *et al.* 2020b).

To provide and establish new synthetic reference glasses whose compositions are closer to natural rocks and minerals, three andesite reference glasses have been prepared (Wu *et al.* 2019). Unlike the soda lime NIST glasses (610, 612, 614 and 616) and basaltic USGS GS synthetic glasses (GSE-1G, GSD-1G, GSC-1G and GSA-1G), this suite of glasses has an andesitic major element composition. These glass reference materials, referred to as the Andesite Glass Reference Materials ARM-1, -2 and -3, were doped with fifty-four trace elements at different levels of 500, 50 and 5 μg g^{-1}. Wu *et al.* (2019) reported the preliminary data for forty-six trace elements using a variety of analytical techniques (EPMA, XRF, ICP-OES, ICP-MS, LA-Q-ICP-MS and LA-SF-ICP-MS) performed in ten different laboratories. It is expected that the ARM glasses will become a useful and important alternative to the widely distributed NIST and USGS GS glasses reference materials for *in situ* microanalysis.

Reference materials are used for measurement of mass fractions, valences (e.g., $Fe^{2+}/\Sigma Fe$ ratio) and isotope ratios (or expressed as delta values) (e.g., Li, B and Pb). For example, *in situ* quantification of $Fe^{2+}/\Sigma Fe$ ratio in natural silicate glasses requires reference materials with known $Fe^{2+}/\Sigma Fe$ values for calibration and/or quality control (Zhang *et al.* 2018a). Currently, the ARM

glasses are only characterised for their mass fractions. To expand the applicability of ARM glasses (ARM-1, -2 and -3) as reference materials for *in situ* microanalysis of isotope ratios and iron oxidation state ($Fe^{2+}/\Sigma Fe$), we measured their Li-B-Si-O-Mg-Sr-Nd-Hf-Pb isotopic compositions and $Fe^{2+}/\Sigma Fe$ values using TIMS, MC-ICP-MS, IR-MS and wet-chemistry colorimetric techniques. The homogeneity of Li-B-O-Nd-Pb isotope ratios at the micro-scale level was evaluated using LA-MC-ICP-MS and SIMS techniques. A previous study presented a limited major element dataset for the ARM glasses (Wu *et al.* 2019). To better constrain and to provide new reference values for the major elements, we report new EPMA data obtained using three different instruments with independent calibrations. The next generation of MC-ICP-MS instruments equipped with a collision/reaction cell has the potential to provide accurate isotope ratios in the presence of large interferences (e.g., $^{87}Rb^{+}$ interference on $^{87}Sr^{+}$). The ARM glasses have high ratios of Rb/Sr, Sm/Nd and Lu/Hf ratios, and could be used as reference materials for calibration and validation purposes.

ARM glass reference materials

The ARM glass reference materials were prepared by directly fusing and stirring 3.8 kg of high-purity oxide powders. Detailed information regarding the preparation and the preliminary characterisation of the ARM glasses is given in Wu *et al.* (2019). *In situ* and bulk analyses indicate these glasses are homogeneous with respect to most element mass fractions (Wu *et al.* 2019). ARM-1, -2 and -3 contain fifty-four trace elements with mass fractions of ~ 500, ~ 50 and ~ 5 μg g^{-1}, respectively, except for arsenic that was used for melt degassing. Although ARM-2 was contaminated with Li, B, Zn and Yb during its preparation, these elements seemed to be homogeneous in the glass.

Analytical techniques

A total of fifteen laboratories from twelve institutions participated in this study: the Institute of Geology and Geophysics, Chinese Academy of Sciences, Beijing, P.R. China (IGGCAS), Leibniz Universität Hannover, Hannover, Germany (LUH), Geowissenschaftliches Zentrum, Universität Göttingen, Göttingen, Germany (GZG), Northwest University, Xi'an, P.R. China (NWU), GFZ German Research Centre for Geosciences, Potsdam, Germany (GFZ), University of Leeds, Leeds, United Kingdom (UL), Istituto di Geoscienze e Georisorse, Consiglio Nazionale delle Ricerche, Pisa, Italy (IGG-CNR), University of Edinburgh, United Kingdom (UE), Institute of Earth and Environment, Chinese Academy of Sciences, Xia'an, P.R. China (IEECAS), University of Science and Technology of China, Anhui, China (USTC), Guangzhou Institute of Geochemistry, Chinese Academy of Sciences, Guangzhou, P.R. China (GIGCAS), University of Geosciences, Hubei, P.R. China (CUG) and Beijing Research Institute of Uranium Geology, Beijing, P.R. China (BRIUG). Table 1 summarises the analysed numbers of samples, analytical techniques and institutions that carried out the analyses. The used methods are described in detail in Appendix S1.

In situ analytical techniques

Electron probe microanalysis: This technique was used for major element determination. The measurements were undertaken on three instruments in two institutions: JEOL JXA 8900Rl (GZG), JXA8100 (IGGCAS) and Cameca SX Five (IGGCAS). All laboratories used StHs6/80-G and ATHO-G (Jochum *et al.* 2006) to assess data quality. Online supporting information Table S1 summarises the instrumental parameters and measurement procedures. Two measurement sessions were performed for each ARM glass at GZG. Each session included fifty spot analyses along a line across a 10 mm × 10 mm surface area. A total of thirty spot analyses for each ARM glass were conducted at IGGCAS. The spots were randomly located on six glass splits, with five spot analyses for each split. A total of fifty spot analyses were conducted on each ARM glass at IGGCAS. Five spot analyses were undertaken on ten randomly selected splits.

LA-MC-ICP-MS: This technique was used to assess the homogeneity of Li-B-Nd-Pb isotope ratios at the micro-scale (~ 100 μm). Lithium, Nd and Pb isotope ratios were measured at

IGGCAS using a 193 nm ArF excimer laser ablation system (Geolas HD, Coherent, Göttingen, Germany) coupled to a Neptune Plus MC-ICP-MS (Thermo Fisher Scientific, Bremen, Germany). The methods are similar to those outlined in Yang *et al.* (2014). For Li, a total of forty spot measurements (equally distributed on ten splits) were conducted on each ARM glass. For Nd, a total of 120 spot measurements (equally distributed on thirty splits) were conducted on ARM-1. For Pb, a total of 100 spot measurements were conducted on each ARM glass. The measurements were equally distributed on twenty-five randomly selected splits. Boron isotope ratios were measured at GIGCAS using a Resolution M50 laser ablation system coupled to a Neptune Plus MC-ICP-MS. The measurement procedures followed those outlined by Zhang *et al.* (2018b). A total of forty spot measurements were undertaken on each ARM glass. The spot measurements were equally distributed in ten randomly selected splits.

SIMS: This technique was used to assess the homogeneity of B and O isotope ratios at the micro-scale (20-30 μm). Oxygen isotope measurements were performed using a CAMECA IMS-1280 SIMS (CAMECA, Gennevilliers, France) at IGGCAS. The measurement procedures followed those outlined by Tang *et al.* (2015, 2020). A single measurement session was carried out for each ARM glass. This session involved forty spot measurements that were equally distributed on twenty randomly selected splits. The B isotope ratios of ARM-1 and ARM-3 were measured using a CAMECA 7f-GEO instrument at UE. One measurement session was carried out with four random measurements on ARM-1 and ARM-3.

Bulk analytical techniques

MC-ICP-MS: This technique was used to determine the Li-B-Si-Mg-Sr-Nd-Hf-Pb isotope ratios of the ARM glasses. The measurements were conducted at seven institutions: GFZ (Li-B), CUG (Li), BRIUG (Li), IGG-CNR (B), USTC (Si), IGGCAS (Mg-Sr-Nd-Hf-Pb) and NWU (Mg-Sr-Nd-Hf-Pb). Table 2 summarises the elemental purification techniques, instrumental settings and the materials used to assess the data quality. At GFZ, the Li and B isotopic compositions of each ARM glass were determined on six or eight chips using a Neptune MC-ICP-MS instrument

(Govindaraju 1994, Romer *et al.* 2014). Lithium and B were analysed on separate splits. At the CUG, two aliquots of each ARM glasses were analysed for Li isotopes using a Neptune Plus MC-ICP-MS. The chemical purification and measurement procedures followed those outlined by Lin *et al.* (2016, 2019b). At BRIUG, single aliquots of each ARM glasses were analysed for Li isotopes using a Nu II MC-ICP-MS (Nu instrument, Wrexham, UK). The chemical purification of Li was carried out using Biorad AG50W-x8 resin. At IGG-CNR, single aliquots of ARM-2 and -3 was analysed for B isotopes using a Neptune Plus MC-ICP-MS. The chemical purification and analytical procedures followed those of previous studies (Tonarini *et al.* 1997, Al-Ammar *et al.* 2000, Guerrot *et al.* 2011). At IEECAS, four aliquots of ARM-2 were analysed for their B isotopic composition using a Neptune Plus MC-ICP-MS. Boron was purified using two different methods, i.e., ion exchange chromatography (He *et al*. 2019) and micro-sublimation (Xiao *et al*. 2019). At USTC, Si isotope ratios of the ARM glasses were determined using a Neptune Plus MC-ICP-MS (Yu *et al.* 2018). Magnesium, Sr, Nd, Hf and Pb isotope ratios were independently analysed at IGGCAS and NWU using Neptune Plus MC-ICP-MS and Nu II MC-ICP-MS instruments, respectively. The detailed chemical and measurement procedures have been described elsewhere (Münker *et al.* 2001, Yang *et al.* 2010, 2011, 2012, 2014, 2020a, 2020b, An *et al.* 2014, Bao *et al.* 2016, 2018, 2019, 2020, Chu *et al.* 2019).

TIMS: This technique was used to measure the Sr-Nd-Pb isotope ratios of the ARM glasses at the IGGCAS. Seven aliquots (for Sr-Nd) and three aliquots (for Pb) of each ARM glasses were measured using a Triton TIMS (Thermo Fisher Scientific, Bremen, Germany). The chemical purification and measurement procedures followed those outlined by Li *et al.* (2016, 2019).

Fluorination techniques for O isotope ratios: These analyses were performed in three institutions: GZG, IGGCAS and USTC. At GZG, the glass samples were reacted with excess BrF_5 in a stainless-steel sample chamber at a pressure of ~ 120 mbar using an infrared laser for heating. The purification of O_2 was undertaken in an in-house developed extraction line comprising of

liquid N_2-based cooling traps and a Hewlett Packard 5890 Series II gas chromatograph with which N_2 was removed from the sample gas at a temperature of 50 °C (Pack *et al.* 2016, Peters *et al.* 2020). The isotope ratio measurements were performed with a ThermoFinnigan MAT 253 gas source isotope ratio mass spectrometer (IRMS). The measured oxygen isotope ratios were normalised to the composition of San Carlos olivine with a $\delta^{18}O = 5.17$ ‰ and a $\Delta'^{17}O = -52$ ppm, where the definition for $\Delta'^{17}O = 1000[\ln(\delta^{17}O/1000+1) + 0.528x(1000\ln(\delta^{18}O/1000+1)]$ is adopted. At IGGCAS, the glass samples were reacted with BrF_5 in a nickel reaction vessel at a temperature of 750 °C for 4 h. The O_2 product was collected in a sample vessel containing a molecular sieve at -196 °C and measured on a ThermoFinnigan 252 IRMS (Tang *et al.* 2019, 2020). At the USTC, O isotope ratios were determined by the laser fluorination method and a ThermoFinnigan Delta XP IRMS. The method is similar to that described by Zheng *et al.* (2002).

Wet chemical analysis of $Fe^{2+}/\Sigma Fe$ ratios: These analyses were performed using two different chemical titration techniques in two institutions: LUH and IGGCAS. At LUH, a wet-chemistry colorimetric method (Schuessler *et al.* 2008), modified after Wilson (1960), was used to analyse the $Fe^{2+}/\Sigma Fe$ ratios. For each analysis, about 10 mg of glass powder was dissolved in a vanadate solution, which was subsequently mixed with H_2SO_4 and HF. After mixing with a quantified ammonium acetate solution and a 2,2′ bipyridine solution, the solution was analysed by UV spectrometry, before and after the addition of a hydroxylamine hydrochloride solution (to convert all Fe to Fe^{2+}). At IGGCAS, glass powders (80–100 mg) were weighed into a PTFE vessel. The powder was digested with H_2SO_4 (50% *v/v*, 10 ml) and HF (5 ml) acid in an Ar atmosphere at on a hot plate of 170 °C surface temperature for 10 min. The ferrous oxide was titrated with a standard potassium permanganate solution. The whole procedure blank was also determined. The detailed method was described by Xue *et al.* (2017).

Results

EPMA major element data

Table 3 lists the new EPMA major element data. The previously published data (Wu *et al.* 2019) are listed for comparison. Most of the new EPMA data are in agreement with the previously published values when the measurement precision (2*s*) is taken into account. The mean FeO fraction obtained using the JXA8100 EPMA at IGCCAS are slightly lower (~ 4%) compared with those from the other EPMA instruments. The new SiO_2 fractions are generally 0.3–1.8% (in relative) higher than the preliminary reference values. The originally published preliminary reference values for SiO_2 (Wu *et al.* 2019) were calculated by averaging data from only two techniques (XRF, $n = 3$; EPMA, $n = 30$). Therefore, the data provided here further constrain the major element compositions of the ARM glasses.

***In situ* Li-B-O-Nd-Pb isotope ratio data**

The *in situ* Li-B-O-Nd-Pb isotope data are summarised in Table S2 and plotted in Figures 1–3. Data for Li, B and O isotope ratios are given as δ-values relative to the commonly used reference materials L-SVEC, NIST SRM 951 and VSMOW2, respectively. The intermediate precision is given as the 2*s* of the mean of multiple spot measurements. The B δ-values and mass fractions by SIMS are included in Appendix S1 (methodology). In general, the intermediate precisions of δ^7Li, δ^{11}B and δ^{18}O for the three ARM glasses are in range of 0.54–2.89‰, 0.57–11.9‰ and 0.18–0.25‰, respectively (Figure 1). The poorer intermediate precision of ARM-3 is due to low signal intensity. A total of 120 ^{143}Nd/^{144}Nd independent measurement results of ARM-1 yielded a mean value of 0.512171 ± 0.000040 (2*s*) (Figure 2). The intermediate precision of Pb isotope ratios from 100 spot measurements of ARM-1, -2 and -3 are in range of 0.13–0.82‰, 0.26–2.07‰ and 0.43–4.03‰, respectively (Figure 3). The difference between the LA-MC-ICP-MS and the bulk solution data is ≤ 1.58‰ for Pb isotope ratios, ≤ 0.34‰ for δ^7Li (except for ARM-2), ≤ 0.29 ‰ for δ^{11}B. The difference between the SIMS and bulk-solution data is ≤ 1.68‰ for δ^{11}B and ≤ 0.28‰ for δ^{18}O (except for ARM-2). These differences are probably due to the matrix effects.

Bulk analytical data

Li-B isotope ratios: Table 4 lists Li and B isotope data for each ARM glass. Three laboratories (CUG, BRIUG and GFZ) determined the δ^7Li values. ARM-1, -2 and -3 yielded overall mean δ^7Li values of 0.46‰ ± 0.31‰ (2*s*, *n* = 9), 0.51‰ ± 0.37‰ (2*s*, *n* = 10) and 3.37‰ ± 0.91‰ (2*s*, *n* = 9), respectively. The slightly higher standard deviation of δ^7Li of ARM-3 glass possibly indicates that this glass is slightly heterogeneous and may show minor variations among different wafers. Three laboratories determined the δ^{11}B values. At GFZ, the δ^{11}B values were determined on six fragments each for ARM-1 and -2 and on eight fragments for ARM-3. ARM-1 and -2 measurements were conducted on the same wafer. Due to its lower B mass fraction, ARM-3 required larger sample size and, therefore, the measurements were conducted on material from two wafers. At IGG-CNR, a single fragment for ARM-2 and ARM-3 was determined for the δ^{11}B values. At IEECAS, the δ^{11}B values of four fragments of sample ARM-2 were determined. The results match well with those from GFZ and IGG-CNR. In summary, ARM-1 and -2 yielded overall mean δ^{11}B values of -11.82‰ ± 0.25‰ (2*s*, *n* = 6) and -12.63‰ ± 0.31‰ (2*s*, *n* = 11), respectively. These two materials appear to be homogeneous on the scale of sampling. While ARM-3 yielded δ^{11}B values ranging from -2.45‰ ± 0.18‰ to -6.77‰ ± 0.25‰ (Table 4).

Oxygen isotope ratios: Table 5 lists the δ^{18}O values for each ARM glass. For ARM-1, the δ^{18}O values obtained from three laboratories are generally in agreement, with a mean value of 5.91‰ ± 0.37‰ (2*s*, *n* = 9). For ARM-2, the δ^{18}O values from USTC are slightly lower than those from the other two laboratories, but within measurement precisions (0.2–0.4‰). For ARM-3, the δ^{18}O values from two laboratories agree well and have an overall mean value of 5.91‰ ± 0.37‰ (2*s*, *n* = 5). The δ^{18}O values obtained by SIMS (calibrated using NIST SRM 610) are systematically lower than the bulk fluorination values, which can probably be attributed to a matrix effect during SIMS measurements. The GZG laboratory reported the δ^{17}O values for the three ARM glasses.

Si-Mg isotope ratios: Data for Si and Mg isotope ratios are given as δ-values relative to the reference materials NBS-28 and DSM3, respectively. Table 6 lists the δ^{30}Si and δ^{29}Si values for the three ARM glasses. The δ^{30}Si and δ^{29}Si values of the three ARM glasses are the same with

mean values of 0.05‰ ± 0.04‰ and 0.04‰ ± 0.02‰ (Table 6). Table 7 lists δ^{25}Mg and δ^{26}Mg values for the three ARM glasses. The results from the two laboratories are in good agreement. The overall mean δ^{26}Mg values for ARM-1, -2 and -3 are -1.12‰ ± 0.03‰ (2*s*, *n* = 5), -1.08‰ ± 0.05‰ (2*s*, *n* = 5) and -1.15‰ ± 0.05‰ (2*s*, *n* = 5), respectively. The negative δ^{26}Mg values of all three ARM glasses were inherited from the starting material (i.e., high-purity MgO powder).

Sr-Nd-Hf isotope ratios: Table 8 lists a compilation of Sr-Nd-Hf isotope ratio data for the three ARM glasses. The Sr isotope ratios for all three ARM glasses were obtained with measurement reproducibility ≤ 39 ppm (2*s*). The overall mean $^{87}Sr/^{86}Sr$ ratios for ARM-1, -2 and -3 are 0.707783 ± 39 (2*s*, *n* = 11), 0.708024 ± 18 (2*s*, *n* = 10) and 0.708810 ± 38 (2*s*, *n* = 12), respectively. For ARM-1, the TIMS value (0.707766 ± 23) appears to be slightly lower than the MC-ICP-MS value (0.707798 ± 21), although these ratios overlap within the estimated precisions. The Nd isotope ratios for the three ARM glasses were obtained with measurement reproducibility ≤ 16 ppm (2*s*). The overall mean $^{143}Nd/^{144}Nd$ ratios of ARM-1, -2 and -3 are 0.512164 ± 13 (2*s*, *n* = 13), 0.512127 ± 13 (2*s*, *n* = 13) and 0.512088 ± 16 (2*s*, *n* = 10). The data obtained by TIMS are in agreement with those obtained by MC-ICP-MS. Two laboratories that used different chemical purification methods and instruments obtained consistent $^{176}Hf/^{177}Hf$ ratios. The overall mean $^{176}Hf/^{177}Hf$ ratios for ARM-1, -2 and -3 are 0.282125 ± 6 (2*s*, *n* = 6), 0.282125 ± 10 (2*s*, *n* = 6) and 0.282136 ± 2 (2*s*, *n* = 3).

Pb isotope ratios: Table 9 lists the Pb isotope ratios determined by TIMS and MC-ICP-MS. ARM-1 and -3 were measured by TIMS (*n* = 3) and MC-ICP-MS (*n* = 6), while ARM-2 was measured with two different MC-ICP-MS instruments and chemical purification procedures. The data obtained by the TIMS and MC-ICP-MS techniques are in good agreement with a bias of 0.1–0.6‰ (in relative). The 2*s* reproducibility is in a range of 0.003–0.023 for $^{206}Pb/^{204}Pb$, $^{207}Pb/^{204}Pb$ and $^{208}Pb/^{204}Pb$, and 0.0004–0.0010 for $^{207}Pb/^{206}Pb$ and $^{208}Pb/^{206}Pb$ ratios. The Pb isotope ratios of three reference glasses show slight differences; $^{207}Pb/^{206}Pb$ = 0.85188 (ARM-2) to 0.85213 (ARM-1) to 0.85071 (ARM-3); $^{207}Pb/^{204}Pb$ =15.667 (ARM-2) to 15.671 (ARM-1) to 15.686 (ARM-3). It

should be mentioned that the data obtained by different methods are not directly comparable as they use different normalisation methods and normalisation materials: TIMS Pb isotope ratio data were corrected for instrumental fractionation using Pb reference material NIST SRM 981 as 'external' reference. MC-ICP-MS Pb isotope ratio data were normalised on-line to the Tl isotopic composition of Tl reference material NIST SRM 997. The used of difference reference materials may be the reason for the minor differences in the data obtained by different techniques.

$Fe^{2+}/\Sigma Fe$ ratios: Table 10 lists the $Fe^{2+}/\Sigma Fe$ ratio data for the three ARM glasses. The $Fe^{2+}/\Sigma Fe$ ratios for each ARM glass were repeatedly measured in three sessions at the LUH, and the results match well with each other within measurement precision. The ARM-1 data obtained at IGGCAS has a slightly higher $Fe^{2+}/\Sigma Fe$ ratio than those from LUH. This is probably due to the relatively large uncertainty, which is related to the oxidation of Fe^{2+} to Fe^{3+} during the measurement process. The mean $Fe^{2+}/\Sigma Fe$ ratios of the three ARM glasses are the same, with a mean value of 0.3. The starting materials for the ARM glasses included the ferric oxide as the Fe source, and the $Fe^{2+}/\Sigma Fe$ value of 0.3 indicates that the ferric oxides was partially reduced during fusion due to the presence of species such as MnO_2 and $NH_4H_2PO_4$, which are as the starting material to produce the glasses.

Discussion

Homogeneity assessment

Homogeneity is a fundamental requirement for any reference material. It is not an inherent property of the material, but is specific to the element and the sample scale. With the new data obtained in this study, we assessed the homogeneity of the ARM glasses with respect to major elements, Li-B-Si-O-Mg-Sr-Nd-Hf-Pb isotope ratios, and $Fe^{2+}/\Sigma Fe$ ratios at the micro- and bulk-scales.

Major elements: The homogeneity of ARM glasses was previously investigated by EPMA of a large glass split (Wu *et al.* 2019). In the present study, their homogeneity was further evaluated by means of EPMA profiles (GZG) and on different glass splits (IGGCAS) (Table S3). The precisions (0.2–2.0%) (2 RSD) for all the ARM glasses are similar to the EPMA repeatability precisions, except for MnO, P_2O_5 and TiO_2. The lower precisions of MnO and P_2O_5 are mainly due to their low mass fractions (< 0.3% *m/m*). These data indicate that possible differences arising from heterogeneity are smaller than the measurement precisions. Figure 4 shows the Al_2O_3 data for the three ARM glasses. The results for two profiles and different glass splits indicate that there are no regions of Al_2O_3 heterogeneity in the analysed ARM glasses. Small variations in Al_2O_3 potentially exist for different splits of ARM-1, but these are generally not significantly larger than the measurement precisions. Figure 4 shows that Al_2O_3 mass fraction data have a Gaussian distribution and thus demonstrate the homogeneity of the ARM glasses.

We used the homogeneity index (*H*; Harries 2014)) to assess the homogeneity of the major element mass fractions. According to Harries (2014), the critical homogeneity (H_{crit}) index is 1.164 for fifty measurements and $\alpha = 0.05$. If the actual homogeneity index is larger than H_{crit}, the heterogeneity is detectable. Figure 5 shows the *H* index of major elements for the three ARM glasses. The results indicate no detectable heterogeneity under the given measurement conditions for most major element mass fractions. However, in the case of K_2O and P_2O_5 there may be some heterogeneity, although it was not reproduced in the two studies. As noted by Harries (2014), this may be due to the spurious rejection of the null hypothesis (5% or 3 of sixty investigated elements). For MnO, two studies yielded a relatively high *H* index that was < 1.5. This may be related to the large measurement precisions, due to the low MnO mass fractions. With this comprehensive homogeneity evaluation, we could clearly demonstrate that all three ARM glasses are homogeneous with respect to major element mass fractions.

Li-B-Si-O-Mg-Sr-Nd-Hf-Pb isotope and $Fe^{2+}/\Sigma Fe$ ratios: The traverses of isotope ratios (Figures 1–3) indicate that there are no regions of large heterogeneity of Li-B-O-Nd-Pb isotope

ratios for any of the ARM glasses. Although some variations do exist, these are generally not significantly greater than the measurement precisions. These variations are mainly restricted to individual measurements, rather than defining a region with a substantially difference of Li-B-O-Nd-Pb isotope ratios. The measured Li-B-O-Nd-Pb isotope ratios show no changes for traverses from different glass splits. The calculated standard deviations of the Li-B-O-Nd-Pb isotope ratios measured for each ARM glasses are similar to the mean of internal standard errors (defined as the "internal precision" 2*s* multiplied by $1/\sqrt{n}$, *n* is the number of cycles of a single analysis.) (Figures 1–3 and Table S1), indicating that any heterogeneity present in the glasses is generally smaller than the intermediate precisions of the LA-MC-ICP-MS and SIMS techniques. However, MC-ICP-MS yielded $\delta^{11}B$ values for ARM-3 ranging from -2.45‰ ± 0.18‰ to -6.77‰ ± 0.25‰ (Table 4) that cannot be explained by the measurement precisions. The B isotopic composition may be heterogeneous in some region of the ARM-3 glass.

For the three ARM glasses, *in situ* evaluation of the homogeneity of Sr-Hf isotope ratios by LA-MC-ICP-MS is hampered by interferences ($^{87}Rb^+$ on $^{87}Sr^+$, $^{176}Lu^+$ and $^{176}Yb^+$ on $^{176}Hf^+$). Therefore, the homogeneity of Sr-Hf isotope ratios was evaluated only on the bulk-scale (i.e., hundreds of mg). Table 8 lists the Sr-Hf isotope data obtained from three instruments. These results indicate that the Sr-Hf isotope ratio data are consistent within measurement uncertainty for the different glass splits. The ARM glasses were produced at a temperature of 1600 °C with continuously stirring over 5 h. Under these conditions, chemical bonds in oxides are broken, and isotopic equilibrium should be achieved. Strontium and Hf are refractory lithophile elements, which are unaffected by volatilisation during melting. A previous study demonstrated the homogeneous distribution of Sr-Hf mass fractions on the micro-scale (Wu *et al.* 2019). As such, the Sr-Hf isotope ratios should be homogeneous on the micro-scale.

The homogeneity of the $Fe^{2+}/\Sigma Fe$ ratios was only evaluated based on bulk solution data (Table 10). The results do not reveal heterogeneity for any of the ARM glasses. The variations are neither generally nor significantly greater than the measurement precisions. The oxygen fugacity of the

melt was uniform because of the continuous stirring during the fusion process. The rapid quenching of the melt (10 s) had a negligible effect on the oxidation states of the glasses. The Fe mass fractions appear to be homogeneous on a micro-scale (10 μm). Therefore, it would be expected that the $Fe^{2+}/\Sigma Fe$ ratios are homogeneous on a micro-scale as well. However, this should be verified using the newly developed EPMA technique for *in situ* measurements of $Fe^{2+}/\Sigma Fe$ ratios (Zhang *et al.* 2018a).

Reference values and their uncertainties

Major elements: The determination of reference values and their uncertainties at the 95% confidence level followed the ISO guidelines (ISO Guide 35 2017) and the Certification Protocol of the International Association of Geoanalysts (Kane *et al.* 2003, 2007). Data quality was checked by careful evaluation and verification of the calibration procedures and analytical techniques. Dixon and Grubbs tests were applied to exclude outliers (Table 3). The statistical parameter W from the Shapiro-Wilk test was calculated for evaluation of a normal distribution. The results indicate that all measurements have normal or nearly normal distributions, except for MnO (Table S4). Therefore, after excluding outliers, the arithmetic mean of the data was taken as the best estimate of the true values. We also assessed the data quality based on the analytical technique used, because the results obtained from each measurement principle (e.g., EPMA, ICP-OES) may show systematic differences. We grouped the data into three categories according to the technique used: ICP-OES, XRF and *in situ* techniques (EPMA and LA-ICP-MS). Table S5 lists the major element mass fractions for each technique category, with the corresponding measurement precisions (expressed as 1*s*). Nearly all analyte mass fraction means agree within uncertainty, indicating that possible systematic differences between the various analytical techniques are absent or small, making a bias component of uncertainty unnecessary.

Reference values are reported if there is data derived from multiple laboratories (p) using independent and well-defined measurement principles that are in statistical agreement (Kane *et al.* 2003, 2007 and personal communications with Thomas Meisel). In order provide a statistically

sound consensus value, $p = 7$ of independent means are required. The major element data meet this requirement. The reference values are comparable to certified values in a certification program. The overall expanded uncertainty U at the 95% confidence level (CL) of the reference values was calculated based on IAG protocol (Kane *et al.* 2003):

$$\mathrm{U} = t \times \mathrm{u} \tag{1}$$

where t is the coverage factor. The Student's t-distribution was used to assign t. Here we used 3 because of the relatively small number of laboratories. According to Kane *et al.* (2003), the uncertainty 'u' is the mainly based on three components of variance that are quadratically combined:

$$u^2 = VAR\left(\frac{Y_{mean}}{\sqrt{p}}\right) + VAR_{inhom} + VAR_{bias} \tag{2}$$

where the first component is the standard deviation of the mean of the n^{th} laboratory data. The second and the third components account for inhomogeneity in the reference materials and inter-laboratory bias, respectively. In this study, the second component is very small and was thus ignored. Biases between the different measurement principles were not observed in the data sets. This means that $VAR_{bias} = 0$.

Table 11 lists the new reference values for major element mass fractions for the three ARM glasses, along with the overall expanded uncertainties at the 95% confidence level (U) and the number values (n) contributing to recommended values. Most data agree within measurement uncertainty with the preliminary reference values of Wu *et al.* (2019). However, the new data are more reliable because more data were used to derive the reference values.

Li-B-Si-O-Mg-Sr-Nd-Hf-Pb isotope and $Fe^{2+}/\Sigma Fe$ ratios: The data quality was carefully checked in different ways (i.e., the calibration procedure and the verification of analytical techniques by measurements of quality control materials) (Table 2). Results obtained by different measurement principles (TIMS and MC-ICP-MS) or one technique from different laboratories are generally in good agreement; therefore no data were identified as outliers. Given the small number of laboratories and/or analyses, it is not possible to calculate reference values following ISO guidelines (ISO Guide 35 2017) and Certification Protocol of the International Association of Geoanalysts (Kane *et al.* 2003, 2007). Therefore, we report the mean values of our data as preliminary reference values. *In situ* techniques (LA-MC-ICP-MS and SIMS) commonly suffer from matrix effects and the data quality are related to the reference material used for calibration Therefore, the preliminary reference values were calculated as the mean values of data obtained by bulk techniques (TIMS, MC-ICP-MS, IRMS and wet-chemistry colorimetry). LA-MC-ICP-MS and SIMS results were excluded from the calculation of mean values for isotope ratios. Table 11 lists the preliminary reference values along with the *p*, 2*s*, 2SE, Cl for Li-B-Si-O-Mg-Sr-Nd-Hf-Pb isotope and $Fe^{2+}/\Sigma Fe$ ratios for the three ARM glasses. The CI and 2SE are only meaningful with $p > 7$. In the case of $p = 1$, the 2*s*, 2SE and Cl could not be calculated and thus marked as "-". In several case of $p = 1$, two laboratories reported identical values, and the 2*s*, 2SE and Cl could not be calculated and thus also marked as "-". The new isotope ratio data provided here will be useful to the geochemical community for *in situ* and bulk analysis, particularly when requesting reference materials with high ratios of Rb/Sr, Sm/Nd and Yb/Hf.

Metrological traceability

Metrological traceability is a key concept in the characterisation of reference materials. It links the validity of all measurement results to national and international reference materials through an unbroken chain of calibrations, each contributing to the measurement uncertainty (Jochum and Enzweiler 2014). Traceability in this study was established by the use of standard solutions and international reference materials. For example, the standard solutions for making calibration curves for ICP-OES analysis were prepared from NIST calibration standard solutions, and the

experimental equipment, scales and measuring instruments were regularly verified or calibrated by certified reference materials. Solid international reference materials were used to establish the traceability of the EPMA. For the bulk techniques, the collaborating laboratories have demonstrated their technical competence in geochemical analytical research, typically by the publications of reports and research papers describing their metrological traceability. Table 2 provides the measured values for quality control materials to further confirm the data quality.

ARM isotope ratio data and a comparison with NIST, MPI-DING and USGS reference glasses

Woodhead and Hergt (2001) showed that the overall Pb isotope ratios of the NIST SRM 610, 612 and 614 glasses is controlled by mixing between the Pb spike and based materials. Baker *et al.* (2004) demonstrated that incomplete mixing appears to have resulted in Pb isotope heterogeneity in NIST SRM 614, even at the tens of mg sampling scale. It is possible to assess the effect of incomplete mixing by comparing the composition of each ARM glass with the mixing lines defined by the compositions of ARM-1 through -3 glass (Kent 2008). Figure 6 shows the Pb isotope ratio relationships between the ARM glasses relative to hypothetical mixing trajectories between the original base glass and trace element spike. ARM-2 deviates from the mixing line because of the contaminations during fusion. This mixing phenomenon between three sources (original base glass, trace element spike and contamination) is also observed for Sr and Nd isotope ratios. For example, with the increasing amounts of spike added to ARM-3 to ARM-1, the $^{87}Sr/^{86}Sr$ ratio decreases from 0.708810 to 0.707783. The uniform Hf isotope ratios indicate that the Hf contributions from the original glass and contamination were generally small.

The NIST and USGS GS reference glasses are synthetic glasses with soda-lime and basaltic matrix compositions. They are commonly used for LA-ICP-MS calibration because of their high and identical trace element mass fractions. Figure 7 shows the $\delta^{7}Li$, $\delta^{11}B$, $\delta^{18}O$, $\delta^{30}Si$ and $\delta^{26}Mg$ values of commonly used NIST, MPI-DING and USGS reference glasses. The data for the MPI-DING and USGS reference glasses were compiled from the literature (Kasemann *et al.* 2001, Le Roux *et*

al. 2004, Jochum *et al.* 2005a, 2006, 2011b, Kasemann *et al.* 2005, Jochum and Nohl 2008, Hartley *et al.* 2012, Lin *et al.* 2014, 2019a, Oeser *et al.* 2014, Schuessler and von Blanckenburg 2014, Frick *et al.* 2016, Kimura *et al.* 2016). Compared with these commercial glasses, the ARM glasses have lower δ^{7}Li, δ^{11}B and δ^{26}Mg values, and higher δ^{30}Si values. The δ^{18}O values of the ARM glasses are similar to the other glasses. Figure 8 compares the Sr-Nd-Hf-Pb isotope ratios of the ARM, NIST and USGS GS glasses. The data for NIST and USGS GS glasses were compiled from previous studies (Baker *et al.* 2004, Jochum and Stoll 2008, Nebel *et al.* 2009, Jochum *et al.* 2011b). Compared with the NIST and USGS GS glasses, the ARM glasses have a relatively narrow range of Pb isotope ratios. The compiled data in Figure 7 and 8 provide a reference for the range of isotope ratios of different established reference materials and the new ARM glasses, and should be aid analysts to choose the appropriate RM for their own studies.

Strontium and Hf isotope ratio data are presented here for each ARM glass. The new generation of MC-ICP-MS instruments with a collision/reaction cell have the potential to remove major isobaric interferences. Thus, it is possible that in the near future, protocols will be developed for *in situ* Sr and Hf isotope ratio measurements of samples with high mass fractions of Rb, Yb and Lu. With the increasing use of multiple ion counters and 10^{13} Ω amplifiers, it is possible to measure isotope ratios for samples with low element mass fractions (< 50 μg g^{-1}) by LA-MC-ICP-MS. The mass fractions of elements in ARM-2 and -3 are relatively low, and these two glasses can be used for the technique development for *in situ* Li, B, Sr, Nd, Hf and Pb isotope ratio measurements of samples with low elemental mass fractions. The ARM glasses are suitable reference materials for instrument calibration, validation of method development and inter-laboratory comparisons.

Availability

Small amounts of ARM glass reference materials can be obtained on request from Key State Laboratory of Lithospheric Evolution, Institute of Geology and Geophysics, China Academy of Sciences (e-mail address: shitou.wu@mail.iggcas.ac.cn)

Conclusions

We have reported Li-B-Si-O-Mg-Sr-Nd-Hf-Pb isotope and $Fe^{2+}/\Sigma Fe$ ratio data for the ARM glass reference materials, as a first approach to providing suitable reference materials for *in situ* isotope ratio measurements by a variety of analytical techniques, such as SIMS, LA-MC-ICP-MS and EPMA. These data were mainly obtained by bulk TIMS, MC-ICP-MS, IRMS and wet-chemistry colorimetric techniques, and were cross-checked by different techniques or laboratories. All three ARM glasses appear to be homogeneous at the scale of sampling volumes and levels of intermediate precision of the utilised techniques. *In situ* Li-B-O-Nd-Pb isotope ratio measurements by LA-MC-ICP-MS and SIMS demonstrated the homogeneity of these isotope ratios at the micron-scale. In addition, we presented new EPMA data for these glasses. Based on published and our new EPMA data, we determined reference values for the major elements and expanded uncertainty (U) at the 95% confidence level following the ISO guidelines and Certification Protocol of the International Association of Geoanalysis. The comprehensive Li-B-Si-O-Mg-Sr-Nd-Hf-Pb isotope and $Fe^{2+}/\Sigma Fe$ ratio data provided here will be useful to the geochemical community for *in situ* microanalysis.

Acknowledgements

Molan Tang and Huan Tian are thanked for their assistance on the calculation of reference values. Two anonymous reviewers are acknowledged for their insightful comments. We are grateful to the editor Thomas Meisel for his constructive comments on the terminology and the guide for the calculation of reference values. This research was supported by the National Natural Science Foundation of China (Grants 41903024 and 41525012)

Data availability statement

References

Al-Ammar A., Reitznerová E. and Barnes R.M. (2000)

Improving boron isotope ratio measurement precision with quadrupole inductively coupled plasma-mass spectrometry. **Spectrochimica Acta Part B, 55,** 1861–1867.

An Y., Wu F., Xiang Y., Nan X., Yu X., Yang J., Yu H., Xie L. and Huang F. (2014)

High-precision Mg isotope analyses of low-Mg rocks by MC-ICP-MS. **Chemical Geology, 390,** 9–21.

Baker J.A., Peate D.W., Waight T.E. and Meyzen C. (2004)

Pb isotopic analysis of standards and samples using a ^{207}Pb-^{204}Pb double spike and thallium to correct for mass bias with a double-focusing MC-ICP-MS. **Chemical Geology, 211,** 275–303.

Bao Z., Huang K.-J., Xu J., Deng L., Yang S., Zhang P. and Yuan H. (2020)

Preparation and characterization of a new reference standard GSB-Mg for Mg isotopic analysis. **Journal of Analytical Atomic Spectrometry, 35,** 1080–1086.

Bao Z., Huang K., Huang T., Shen B., Zong C., Chen K. and Yuan H. (2019)

Precise magnesium isotope analyses of high-K and low-Mg rocks by MC-ICP-MS. **Journal of Analytical Atomic Spectrometry, 34,** 940–953.

Bao Z., Yuan H., Zong C., Liu Y., Chen K. and Zhang Y. (2016)

Simultaneous determination of trace elements and lead isotopes in fused silicate rock powders using a boron nitride vessel and fsLA-(MC)-ICP-MS. **Journal of Analytical Atomic Spectrometry, 31,** 1012–1022.

Bao Z., Zong C., Fang L., Yuan H., Chen K. and Dai M.J.A.G. (2018)

Determination of Hf–Sr–Nd isotopic ratios by MC-ICP-MS using rapid acid digestion after flux-free fusion in geological materials. **Acta Geochimica, 37,** 244–256.

Chu Z.-Y., Wang M.-J., Li C.-F., Yang Y.-H., Xu J.-J., Wang W. and Guo J.-H. (2019)

Separation of Nd from geological samples by a single TODGA resin column for high precision Nd isotope analysis as NdO^+ by TIMS. **Journal of Analytical Atomic Spectrometry, 34,** 2053–2060.

Denton J., Murrell M., Goldstein S., Nunn A., Amato R. and Hinrichs K. (2013)

Evaluation of new geological reference materials for uranium-series measurements: Chinese Geological Standard Glasses (CGSG) and macusanite obsidian. **Analytical Chemistry, 85,** 9975–9981.

Elburg M., Vroon P., van der Wagt B. and Tchalikian A. (2005)

Sr and Pb isotopic composition of five USGS glasses (BHVO-2G, BIR-1G, BCR-2G, TB-1G, NKT-1G). **Chemical Geology, 223,** 196–207.

Frick D.A., Schuessler J.A. and von Blanckenburg F. (2016)

Development of routines for simultaneous *in situ* chemical composition and stable Si isotope ratio analysis by femtosecond laser ablation inductively coupled plasma-mass spectrometry. **Analytica Chimica Acta, 938,** 33–43.

Govindaraju K. (1994)

1994 compilation of working values and sample description for 383 geostandards. **Geostandards Newsletter, 18 (Special Issue)**, 158pp.

Guerrot C., Millot R., Robert M. and Négrel P. (2011) Accurate and high-precision determination of boron isotopic ratios at low concentration by MC-ICP-MS (Neptune) **Geostandards and Geoanalytical Research, 35,** 275–284.

Guillong M., Hametner K., Reusser E., Wilson S.A. and Günther D. (2005)

Preliminary characterisation of new glass reference materials (GSA-1G, GSC-1G, GSD-1G and GSE-1G) by laser ablation-inductively coupled plasma-mass spectrometry using 193 nm, 213 nm and 266 nm wavelengths **Geostandards and Geoanalytical Research, 29,** 315–331.

Harries D. (2014)

Homogeneity testing of microanalytical reference materials by electron probe microanalysis (EPMA). **Chemie der Erde-Geochemistry, 74,** 375–384.

Hartley M., Thordarson T., Taylor C. and Fitton J. (2012)

Evaluation of the effects of composition on instrumental mass fractionation during SIMS oxygen isotope analyses of glasses. **Chemical Geology, 334,** 312–323.

He M.-Y., Deng L., Lu H. and Jin Z.-D. (2019)

Elimination of boron memory effect for rapid and accurate boron isotope analysis by MC-ICP-MS using NaF. **Journal of Analytical Atomic Spectrometry, 34,** 1026–1032

Hu M.Y., Fan X.T., Stoll B., Kuzmin D., Liu Y., Liu Y.S., Sun W.D., Wang G., Zhan X.C. and Jochum K.P. (2011)

Preliminary characterisation of new reference materials for microanalysis: Chinese Geological Standard Glasses CGSG-1, CGSG-2, CGSG-4 and CGSG-5. **Geostandards and Geoanalytical Research, 35,** 235–251.

Huang C., Wang H., Yang J.-H., Ramezani J., Yang C., Zhang S.-B., Yang Y.-H., Xia X.-P., Feng L.-J., Lin J., Wang T.-T., Ma Q., He H.-Y., Xie L.-W. and Wu S.-T. (2020)

SA01 – A proposed zircon reference material for microbeam U-Pb Age and Hf-O isotopic determination. **Geostandards and Geoanalytical Research, 44,** 103–123.

Ibanez-Mejia M., Gehrels G.E., Ruiz J., Vervoort J.D., Eddy M.P. and Li C. (2014)

Small-volume baddeleyite (ZrO_2) U–Pb geochronology and Lu–Hf isotope geochemistry by LA-ICP-MS. Techniques and applications. **Chemical Geology, 384,** 149–167.

ISO 17034 Guide 35 (2017)

Reference materials – Guidance for characterization and assessment of homogeneity and stability (4th edition). **International Organisation for Standardization (Geneva),** 105pp.

Jochum K.P., Dingwell D.B., Rocholl A., Stoll B., Hofmann A.W., Becker S., Besmehn A., Bessette D., Dietze H.J. and Dulski P. (2000)

The preparation and preliminary characterisation of eight geological MPI-DING reference glasses for *in-situ* microanalysis. **Geostandards Newsletter: The Journal of Geostandards and Geoanalysis, 24,** 87–133.

Jochum K.P. and Enzweiler J. (2014)

Reference materials in geochemical and environmental research. **Treatise on Geochemistry (Second Edition). Elsevier (Oxford),** 43–70.

Jochum K.P. and Nohl U. (2008)

Reference materials in geochemistry and environmental research and the GeoReM database. **Chemical Geology, 253,** 50–53.

Jochum K.P., Nohl U., Herwig K., Lammel E., Stoll B. and Hofmann A.W. (2005a)

GeoReM: A new geochemical database for reference materials and isotopic standards. **Geostandards and Geoanalytical Research, 29,** 333–338.

Jochum K.P. and Stoll B. (2008)

Reference materials for elemental and isotopic analyses by LA-(MC)-ICP-MS: Successes and outstanding needs. **In: Laser Ablation ICP-MS in the Earth Sciences: Current practices and outstanding issues. The Canadian Mineralogist, 40,** 147–168.

Jochum K.P., Stoll B., Herwig K., Willbold M., Hofmann A.W., Amini M., Aarburg S., Abouchami W., Hellebrand E., Mocek B., Raczek I., Stracke A., Alard O., Bouman C., Becker S., Dücking M., Brätz H., Klemd R., de Bruin D., Canil D., Cornell D., de Hoog C.-J., Dalpé C., Danyushevsky L., Eisenhauer A., Gao Y., Snow

J.E., Groschopf N., Günther D., Latkoczy C., Guillong M., Hauri E.H., Höfer H.E., Lahaye Y., Horz K., Jacob D.E., Kasemann S.A., Kent A.J.R., Ludwig T., Zack T., Mason P.R.D., Meixner A., Rosner M., Misawa K., Nash B.P., Pfänder J., Premo W.R., Sun W.D., Tiepolo M., Vannucci R., Vennemann T., Wayne D. and Woodhead J.D. (2006)

MPI-DING reference glasses for *in situ* microanalysis: New reference values for element concentrations and isotope ratios. **Geochemistry, Geophysics, Geosystems, 7,** 1–44.

Jochum K.P., Weis U., Stoll B., Kuzmin D., Yang Q.C., Raczek I., Jacob D.E., Stracke A., Birbaum K., Frick D.A., Günther D. and Enzweiler J. (2011a)

Determination of reference values for NIST SRM 610–617 glasses following ISO guidelines. **Geostandards and Geoanalytical Research, 35,** 397–429.

Jochum K.P., Willbold M., Raczek I., Stoll B. and Herwig K. (2005b)

Chemical characterisation of the USGS reference glasses GSA-1G, GSC-1G, GSD-1G, GSE-1G, BCR-2G, BHVO-2G and BIR-1G using EPMA, ID-TIMS, ID-ICP-MS and LA-ICP-MS. **Geostandards and Geoanalytical Research, 29,** 285–302.

Jochum K.P., Wilson S.A., Abouchami W., Amini M., Chmeleff J., Eisenhauer A., Hegner E., Iaccheri L.M., Kieffer B., Krause J., McDonough W.F., Mertz-Kraus R., Raczek I., Rudnick R.L., Scholz D., Steinhoefel G., Stoll B., Stracke A., Tonarini S., Weis D., Weis U. and Woodhead J.D. (2011b)

GSD-1G and MPI-DING reference glasses for *in situ* and bulk isotopic determination. **Geostandards and Geoanalytical Research, 35,** 193–226.

Kane J.S., Potts P.J., Meisel T. and Wiedenbeck M. (2007)

International Association of Geoanalysts' protocol for the certification of geological and environmental reference materials: A supplement. **Geostandards and Geoanalytical Research, 31,** 285–288.

Kane J.S., Potts P.J., Wiedenbeck M., Carignan J. and Wilson S. (2003)

International Association of Geoanalysts' protocol for the certification of geological and environmental reference materials. **Geostandards Newsletter: The Journal of Geostandards and Geoanalysis, 27,** 227–244.

Kasemann S., Meixner A., Rocholl A., Vennemann T., Rosner M., Schmitt A.K. and Wiedenbeck M. (2001)

Boron and oxygen isotope composition of certified reference materials NIST SRM 610/612 and reference materials JB-2 and JR-2. **Geostandards Newsletter: The Journal of Geostandards and Geoanalysis, 25,** 405–416.

Kasemann S.A., Jeffcoate A.B. and Elliott T. (2005)

Lithium isotope composition of basalt glass reference material. **Analytical Chemistry, 77,** 5251–5257.

Kent A.J.R. (2008)

Lead isotope homogeneity of NIST SRM 610 and 612 glass reference materials: Constraints from laser ablation multicollector ICP-MS (LA-MC-ICP-MS) analysis. **Geostandards and Geoanalytical Research, 32,** 129–147.

Kimura J.-I., Chang Q., Ishikawa T. and Tsujimori T. (2016)

Influence of laser parameters on isotope fractionation and optimisation of lithium and boron isotope ratio measurements using laser ablation-multiple Faraday collector-inductively coupled plasma-mass spectrometry. **Journal of Analytical Atomic Spectrometry, 31,** 2305–2320.

Le Roux P., Shirey S., Benton L., Hauri E. and Mock T. (2004)

In situ, multiple-multiplier, laser ablation ICP-MS measurement of boron isotopic composition ($\delta^{11}B$) at the nanogram level. **Chemical Geology, 203,** 123–138.

Li C.-F., Wang X.-C., Guo J.-H., Chu Z.-Y. and Feng L.-J. (2016)

Rapid separation scheme of Sr, Nd, Pb, and Hf from a single rock digest using a tandem chromatography column prior to isotope ratio measurements by mass spectrometry. **Journal of Analytical Atomic Spectrometry, 31,** 1150–1159.

Li C.-F., Wu H.-Q., Chu Z.-Y., Wang X.-C., Li Y.-L. and Guo J.-H. (2019)

Precise determination of radiogenic Sr and Nd isotopic ratios and Rb, Sr, Sm, Nd elemental concentrations in four coal ash and coal fly ash reference materials using isotope dilution thermal ionization mass spectrometry. **Microchemical Journal, 146,** 906–913.

Lin J., Liu Y., Hu Z., Chen W., Zhang C.x., Zhao K. and Jin X. (2019a)

Accurate analysis of Li isotopes in tourmalines by LA-MC-ICP-MS under "wet" conditions with non-matrix-matched calibration. **Journal of Analytical Atomic Spectrometry, 34,** 1145–1153.

Lin J., Liu Y., Hu Z., Chen W., Zhang L. and Chen H. (2019b)

Accurate measurement of lithium isotopes in eleven carbonate reference materials by MC-ICP-MS with soft extraction mode and 10^{12} Ω resistor high-gain Faraday amplifiers. **Geostandards and Geoanalytical Research, 43,** 277–289.

Lin J., Liu Y., Hu Z., Yang L., Chen K., Chen H., Zong K. and Gao S (2016)

Accurate determination of lithium isotope ratios by MC-ICP-MS without strict matrix-matching by using a novel washing method. **Journal of Analytical Atomic Spectrometry, 31,** 390–397.

Lin L., Hu Z., Yang L., Zhang W., Liu Y., Gao S. and Hu S. (2014)

Determination of boron isotope compositions of geological materials by laser ablation MC-ICP-MS using newly designed high sensitivity skimmer and sample cones. **Chemical Geology, 386,** 22–30.

Liu Y., Li X.-H., Li Q.-L. and Tang G.-Q. (2020)

Breakthrough of 2- to 3-μm scale U–Pb zircon dating using Cameca IMS-1280HR SIMS. **Surface and Interface Analysis, 52,** 214–223.

Liu Y., Li X.-H., Li Q.-L., Tang G.-Q. and Yin Q.-Z. (2011)

Precise U–Pb zircon dating at a scale of < 5 micron by the CAMECA 1280 SIMS using a Gaussian illumination probe. **Journal of Analytical Atomic Spectrometry, 26,** 845–851.

Münker C., Weyer S., Scherer E. and Mezger K. (2001)

Separation of high field-strength elements (Nb, Ta, Zr, Hf) and Lu from rock samples for MC-ICP-MS measurements. **Geochemistry, Geophysics, Geosystems, 2,** 1–19.

Nebel O., Morel M.L. and Vroon P.Z. (2009)

Isotope dilution determinations of Lu, Hf, Zr, Ta and W, and Hf isotope compositions of NIST SRM 610 and 612 glass wafers. **Geostandards and Geoanalytical Research, 33,** 487–499.

Oeser M., Weyer S., Horn I. and Schuth S. (2014)

High-precision Fe and Mg isotope ratios of silicate reference glasses determined *in situ* by femtosecond LA-MC-ICP-MS and by solution nebulisation MC-ICP-MS. **Geostandards and Geoanalytical Research, 38,** 311–328.

Pack A., Tanaka R., Hering M., Sengupta S., Peters S. and Nakamura E. (2016)

The oxygen isotope composition of San Carlos olivine on the VSMOW2-SLAP2 scale. **Rapid Communications in Mass Spectrometry, 30,** 1495–1504.

Pearce N.J.G., Perkins W.T., Westgate J.A., Gorton M.P., Jackson S.E., Neal C.R. and Chenery S.P. (1997)

A compilation of new and published major and trace element data for NIST SRM 610 and NIST SRM 612 glass reference materials. **Geostandards Newsletter: The Journal of Geostandards and Geoanalysis, 21,** 115–144.

Peters S.T., Szilas K., Sengupta S., Kirkland C.L., Garbe-Schönberg D. and Pack A. (2020)

> 2.7 Ga metamorphic peridotites from southeast Greenland record the oxygen isotope composition of Archean seawater. **Earth and Planetary Science Letters, 544,** 116331.

Rocholl A.B.E., Simon K., Jochum K.P., Bruhn F., Gehann R., Kramar U., Luecke W., Molzahn M., Pernicka E., Seufert M., Spettel B. and Stummeier J. (1997)

Chemical characterisation of NIST silicate glass certified reference material SRM 610 by ICP-MS, TIMS, LIMS, SSMS, INAA, AAS and PIXE. **Geostandards Newsletter-the Journal of Geostandards and Geoanalysis, 21,** 101–114.

Romer R.L., Meixner A. and Hahne K. (2014)

Lithium and boron isotopic composition of sedimentary rocks – The role of source history and depositional environment: A 250 Ma record from the Cadomian orogeny to the Variscan orogeny. **Gondwana Research, 26,** 1093–1110.

Schuessler J.A., Botcharnikov R.E., Behrens H., Misiti V. and Freda C. (2008)

Amorphous materials: Properties, structure and durability: Oxidation state of iron in hydrous phono-tephritic melts. **American Mineralogist, 93,** 1493–1504.

Schuessler J.A. and von Blanckenburg F. (2014)

Testing the limits of micro-scale analyses of Si stable isotopes by femtosecond laser ablation multicollector inductively coupled plasma-mass spectrometry with application to rock weathering. **Spectrochimica Acta Part B, 98,** 1–18.

Sylvester P.J. and Jackson S.E. (2016)

A brief history of laser ablation inductively coupled plasma-mass spectrometry (LA-ICP-MS). **Elements, 12,** 307–310.

Tang G.-Q., Li X.-H., Li Q., Li Y., Ling X.-X. and Yin Q.-Z. (2015)

Deciphering physical mechanism of topography effect for oxygen isotope measurements using Cameca IMS-1280 SIMS. **Journal of Analytical Atomic Spectrometry, 30,** 950–956.

Tang G.-Q., Liu Y., Li Q.-L., Feng L.-J., Wei G.-J., Su W., Li Y., Ren G.-H. and Li X.-H. (2020)

New natural and fused quartz reference materials for oxygen isotope microanalysis. **Atomic Spectroscopy, 41,** 188–

193.

Tang G.Q., Su B.X., Li Q.L., Xia X.P., Jing J.J., Feng L.J., Martin L., Yang Q. and Li X.H. (2019)

High-Mg# olivine, clinopyroxene and orthopyroxene reference materials for *in situ* oxygen isotope determination. **Geostandards and Geoanalytical Research, 43,** 585–593.

Tonarini S., Pennisi M. and Leeman W.P. (1997)

Precise boron isotopic analysis of complex silicate (rock) samples using alkali carbonate fusion and ion-exchange separation. **Chemical Geology, 142,** 129–137.

Wilson A.D. (1960)

The micro-determination of ferrous iron in silicate minerals by a volumetric and a colorimetric method. **Analyst, 85,** 823–827.

Woodhead J.D. (2002)

A simple method for obtaining highly accurate Pb isotope data by MC-ICP-MS. **Journal of Analytical Atomic Spectrometry, 17,** 1381–1385.

Woodhead J.D. and Hergt J.M. (2001)

Strontium, neodymium and lead isotope analyses of NIST glass certified reference materials: SRM 610, 612, 614. **Geostandards Newsletter: The Journal of Geostandards and Geoanalysis, 25,** 261–266.

Woodhead J.D., Horstwood M.S. and Cottle J.M. (2016)

Advances in isotope ratio determination by LA-ICP-MS. **Elements, 12,** 317–322.

Wu S., Wörner G., Jochum K.P., Stoll B., Simon K. and Kronz A. (2019)

The preparation and preliminary characterisation of three synthetic andesite reference glass materials (ARM-1, ARM-2, ARM-3) for *in situ* microanalysis. **Geostandards and Geoanalytical Research, 43,** 567–584.

Wu S., Yang M., Yang Y., Xie L., Huang C., Wang H. and Yang J. (2020)

Improved *in situ* zircon U–Pb dating at high spatial resolution (5–16 μm) by laser ablation-single collector-sector field-ICP-MS using Jet sample and X skimmer cones. **International Journal of Mass Spectrometry, 456,** 116394.

Xiao J., Vogl J., Rosner M., Deng L. and Jin Z.-D. (2019)

A validated analytical procedure for boron isotope analysis in plants by MC-ICP-MS. **Talanta, 196,** 389–394.

Xie L.-W., Yang J.-H., Yin Q.-Z., Yang Y.-H., Liu J. and Huang C. (2017)

High spatial resolution *in situ* U-Pb dating by laser ablation multiple ion counting collector inductively coupled plasma-mass spectrometry (LA-MIC-ICP-MS). **Journal of Analytical Atomic Spectrometry, 32,** 975–986.

Xue D., Wang H., Liu Y., Xie L. and Shen P. (2017)

An improved procedure for the determination of ferrous iron mass fraction in silicate rocks using a Schlenk Line-based digestion apparatus to exclude oxygen. **Geostandards and Geoanalytical Research, 41,** 411–425.

Yang M., Yang Y.-H., Evans N.J., Xie L.-W., Huang C., Wu S.-T., Yang J.-H. and Wu F.Y. (2020a)

Precise and accurate determination of Lu and Hf contents, and Hf isotopic compositions in Chinese rock reference materials by MC-ICP-MS. **Geostandards and Geoanalytical Research, 44,** 553–565.

Yang Y.-H., Chu Z.-Y., Wu F.-Y., Xie L.-W. and Yang J.-H. (2011)

Precise and accurate determination of Sm, Nd concentrations and Nd isotopic compositions in geological samples by MC-ICP-MS. **Journal of Analytical Atomic Spectrometry, 26,** 1237–1244.

Yang Y.-H., Wu F.-Y., Liu Z.-C., Chu Z.-Y., Xie L.-W. and Yang J.-H. (2012)

Evaluation of Sr chemical purification technique for natural geological samples using common cation-exchange and Sr-specific extraction chromatographic resin prior to MC-ICP-MS or TIMS measurement. **Journal of Analytical Atomic Spectrometry, 27,** 516–522.

Yang Y.-H., Wu F.-Y., Yang J.-H., Chew D.M., Xie L.-W., Chu Z.-Y., Zhang Y.-B. and Huang C. (2014)

Sr and Nd isotopic compositions of apatite reference materials used in U–Th–Pb geochronology. **Chemical Geology, 385,** 35–55.

Yang Y.-H., Yang M., Jochum K.P., Wu S.-T., Zhao H., Xie L.-W., Huang C., Zhan X.-C., Yang J.-H. and Wu F.-Y. (2020b)

High-precision Sr-Nd-Hf-Pb isotopic composition of Chinese Geological Glass Reference Materials CGSG-1, CGSG-2, CGSG-4 and CGSG-5 by MC-ICP-MS and TIMS. **Geostandards and Geoanalytical Research, 44,** 567–579.

Yang Y.-H., Zhang H.-F., Chu Z.-Y., Xie L.-W. and Wu F.-Y. (2010)

Combined chemical separation of Lu, Hf, Rb, Sr, Sm and Nd from a single rock digest and precise and accurate isotope determinations of Lu–Hf, Rb–Sr and Sm–Nd isotope systems using multi-collector ICP-MS and TIMS. **International Journal of Mass Spectrometry, 290,** 120–126.

Yu H.-M., Li Y.-H., Gao Y.-J., Huang J. and Huang F. (2018)

Silicon isotopic compositions of altered oceanic crust: Implications for Si isotope heterogeneity in the mantle. **Chemical Geology, 479,** 1–9.

Zhang C., Almeev R.R., Hughes E.C., Borisov A.A., Wolff E.P., Höfer H.E., Botcharnikov R.E. and Koepke J. (2018a)

Electron microprobe technique for the determination of iron oxidation state in silicate glasses. **American Mineralogist, 103,** 1445–1454.

Zhang W., Chen H., Peng L., Zhao L., Huang J., Lu W., Liang P. and Lai C. (2018b)

Discriminating hydrothermal fluid sources using tourmaline boron isotopes: Example from Bailingshan Fe deposit in the Eastern Tianshan, NW China. **Ore Geology Reviews, 98,** 28–37.

Zheng Y.-F., Wang Z.-R., Li S.-G. and Zhao Z.-F. (2002)

Oxygen isotope equilibrium between eclogite minerals and its constraints on mineral Sm-Nd chronometer.

Geochimica et Cosmochimica Acta, 66, 625–634.

Supporting Information

The following supporting information may be found in the online version of this article:

Appendix S1. Methodology of the twenty laboratories.

Table S1. Summary of the EPMA instrumental parameters and analytical procedures.

Table S2. *In situ* Li-B-O-Nd-Pb isotope data for the ARM-1, -2 and -3 glasses.

Table S3. EPMA major element data.

Table S4. Results of Shapiro-Wilk test.

Table S5. Mean data for each technique (ICP-OES, XRF and *in situ* techniques).

This material is available from: http://onlinelibrary.wiley.com/doi/10.1111/ggr.00000/abstract (This link will take you to the article abstract).

Figure captions

Figure 1. *In situ* δ^{7}Li, δ^{11}B, and δ^{18}O data for the ARM-1, -2 and -3 glasses for the homogeneity study. δ^{7}Li and δ^{11}B data were obtained by LA-MC-ICP-MS and δ^{18}O data were obtained by SIMS. A total of ten splits were analysed for each ARM glass. Four randomly selected spots were

analysed for each split. The "mean value ± 2*s*" was calculated based on forty individual measurement results. The grey field represents the 2*s* range.

Figure 2. LA-MC-ICP-MS $^{143}Nd/^{144}Nd$ data for ARM-1. A total of twenty-four splits were analysed. Five randomly selected spots were analysed for each split. The "mean value ± 2*s*" was calculated based on 120 individual measurement results. The grey zone represents the 2*s* range.

Figure 3. Plots of LA-MC-ICP-MS $^{207}Pb/^{206}Pb$ and $^{207}Pb/^{204}Pb$ data for the ARM-1, -2 and -3 glasses. A total of twenty-five splits were analysed for each ARM glass. For each split, four randomly selected spots were analysed. "- ‰" is the intermediate precision the measurement results expressed as 2 RSD (relative standard deviation), which was calculated from 100 individual measurements. The "mean value ± 2*s*" was calculated based on 100 measurements. The grey field represents the 2*s* range. The bulk solution values are shown and plotted as red lines for comparison.

Figure 4. Plots of EPMA data (from GZG and IGGCAS) for Al_2O_3 in the ARM-1, -2 and -3 glasses. "- ‰" is the 2 RSD (relative standard deviation), which was calculated from the corresponding numbers of measurement results. Histograms of the measurement results plotted next to the data profiles indicate a Gaussian distribution, demonstrating that measurement precision resulted from counting statistics rather than sample heterogeneity.

Figure 5. Homogeneity (*H*) index for major elements in ARM-1, -2 and -3 glasses. The data are from two measurement sessions at the GZG laboratory. $H_{crit} = 1.164$ and $H = 1.5$ are plotted. H_{crit} represents the critical homogeneity index. If the actual homogeneity index is larger than H_{crit}, then heterogeneity is detectable.

Figure 6. Plot of $^{207}Pb/^{204}Pb$ vs. $^{206}Pb/^{204}Pb$ ratios for ARM-1, -2 and -3 glasses showing mixing between the base glass and the spikes. The ARM-2 data deviate slightly from the mixing line,

which is possibly due to the contaminations during glass preparation.

Figure 7. Comparison of δ^{7}Li, δ^{11}B, δ^{18}O, δ^{30}Si and δ^{26}Mg for ARM, NIST, MPI-DING and USGS reference glasses. The reference values for the NIST, MPI-DING and USGS glasses were taken from the literature (Kasemann *et al.* 2001, Le Roux *et al.* 2004, Jochum *et al.* 2005a, 2006, 2011b, Kasemann *et al.* 2005, Jochum and Nohl 2008, Hartley *et al.* 2012, Lin *et al.* 2014, 2019a, Oeser *et al.* 2014, Schuessler and von Blanckenburg 2014, Frick *et al.* 2016, Kimura *et al.* 2016).

Figure 8. Plots showing the differences in Sr-Nd-Hf-Pb isotopic ratios for ARM, NIST and USGS GS glasses. The Sr-Nd-Hf-Pb isotope ratio data for the NIST and USGS GS glasses were taken from the literature (Baker *et al.* 2004, Jochum and Stoll 2008, Nebel *et al.* 2009, Jochum *et al.* 2011b).

Table 1.

Summary of the measured isotopes, numbers of samples, techniques and institutions

	Technique	Samples (analysed number)	Instrumentation	Institute
***In situ* analysis**				
Major elements	EPMA	ARM-1 (100), ARM-2 (100), ARM-3 (100)	JEOL JXA 8900Rl	GZG
	EPMA	ARM-1 (30), ARM-2 (30), ARM-3 (30)	JEOL JXA 8100	IGGCAS
	EPMA	ARM-1 (50), ARM-2 (50), ARM-3 (50)	Cameca SX Five	IGGCAS
Li	LA-MC-ICP-MS	ARM-1 (40), ARM-2 (40), ARM-3 (40)	Geolas HD + Neptune Plus	IGGCAS
B	LA-MC-ICP-MS	ARM-1 (40), ARM-2 (40), ARM-3 (40)	Resolution M50 + Neptune Plus	GIGCAS
	SIMS	ARM-1 (4), ARM-3 (4)	Cameca 7f-GEO	UE
O	SIMS	ARM-1 (40), ARM-2 (40), ARM-3 (40)	Cameca 1280HR	IGGCAS
Nd	LA-MC-ICP-MS	ARM-1 (100)	Geolas HD + Neptune Plus	IGGCAS
Pb	LA-MC-ICP-MS	ARM-1 (100), ARM-2 (100), ARM-3 (100)	Geolas HD + Neptune Plus	IGGCAS
Bulk analysis				
Li	MC-ICP-MS	ARM-1 (6), ARM-2 (6), ARM-3 (6)	Neptune	GFZ
	MC-ICP-MS	ARM-1 (2), ARM-2 (2), ARM-3 (2)	Neptune Plus	CUG
	MC-ICP-MS	ARM-1 (1), ARM-2 (1), ARM-3 (1)	Nu 2	BRIUG

B	MC-ICP-MS	ARM-1 (6), ARM-2 (6), ARM-3 (8)	Neptune	GFZ
	MC-ICP-MS	ARM-2 (1), ARM-3 (1)	Neptune Plus	IGG-CNR
	MC-ICP-MS	ARM-2 (4)	Neptune Plus	IEECAS
Si	MC-ICP-MS	ARM-1 (2), ARM-2 (2), ARM-3 (2)	Neptune Plus	USTC
O	Laser fluorination	ARM-1 (2), ARM-2 (2), ARM-3 (2)	MAT253	GZG
	Nickel Reaction Vessel	ARM-1 (3), ARM-2 (3), ARM-3 (3)	MAT253	IGGCAS
	Laser fluorination	ARM-1 (4), ARM-2 (4)	MAT252	USTC
Mg	MC-ICP-MS	ARM-1 (2), ARM-2 (2), ARM-3 (2)	Neptune Plus	IGGCAS
	MC-ICP-MS	ARM-1 (3), ARM-2 (3), ARM-3 (3)	Nu 2	NWU
Sr	TIMS	ARM-1 (7), ARM-2 (7), ARM-3 (7)	Triton	IGGCAS
	MC-ICP-MS	ARM-1 (3), ARM-2 (3), ARM-3 (3)	Neptune Plus	IGGCAS
	MC-ICP-MS	ARM-1 (3), ARM-2 (3), ARM-3 (3)	Nu 2	NWU
Nd	TIMS	ARM-1 (7), ARM-2 (7), ARM-3 (7)	Triton	IGGCAS
	MC-ICP-MS	ARM-1 (3), ARM-2 (3), ARM-3 (3)	Neptune Plus	IGGCAS
	MC-ICP-MS	ARM-1 (3), ARM-2 (3), ARM-3 (3)	Nu 2	NWU
Hf	MC-ICP-MS	ARM-1 (3), ARM-2 (3),	Neptune Plus	IGGCAS

		ARM-3 (3)		
	MC-ICP-MS	ARM-1 (3), ARM-2 (3)	Nu 2	NWU
	TIMS	ARM-1 (3), ARM-3 (3)	Triton	IGGCAS
Pb				

Table 2.

Instrument parameters, measurement conditions, calibration procedures, calibration standard solutions and quality control materials used for TIMS and MC-ICP-MS analyses. The results for calibration standard solutions and quality control materials are also listed. For the IEECAS, data annotated with the superscripts "1" and "2" refer to the purification technique "ion exchange chromatography" and "micro-sublimation", respectively

Laboratory	**GFZ**	**CUG**	**BIRUG**	**IGG-CNR**	**IEECAS**	**USTC**	**IGGCAS**	**IGGCAS**	**NWU**
Instrumentation	MC-ICP-MS	MC-ICP-MS	MC-ICP-MS	MC-ICP-MS	MC-ICP-MS	MC-ICP-MS	TIMS	MC-ICP-MS	MC-ICP-MS
Make, mode, and type	Thermo Scientific Neptune	Thermo Scientific Neptune Plus	Nu Instrument Nu II	Thermo Scientific Neptune Plus	Thermo Scientific Neptune Plus	Thermo Scientific Neptune Plus	Thermo Scientific Triton Plus	Thermo Scientific Neptune Plus	Nu Instrument Nu II
Measured isotopes and duplicate numbers	Li (n = 6) B (n = 6 or 8)	Li (n = 3)	Li (n = 1)	B (n = 1)	B (n = 2)	Si (n = 2)	Sr-Nd (n = 7) Pb (n = 3)	Mg (n = 2) Sr-Nd-Hf-Pb (n = 3)	Mg-Sr-Nd-Hf-Pb (n = 3)
Sample decomposition	PTFE vessels HF (Li)	PTFE vessels $HF\text{-}HNO_3\text{-}HClO$	PTFE vessels	K_2CO_3 alkaline	PTFE vessels $HF\text{-}HNO_3$	NaOH alkali fusion	Savillex screw-cap beaker	Savillex screw-cap beaker	Bomb $HF\text{-}HNO_3\text{-}HClO_4$

	K_2CO_3 alkaline fusion (B) two-stage Biorad AG 50W-x8 resin for Li; Two-step Amberlite IRA743 and Biorad AG50W-x8 resin for B	$_4$	$HF-HNO_3$	fusion			$HF-HNO_3$	$HF-HNO_3-HClO_4$	
Chemical Purification		Single-stage AG50W-x8	Single-stage AG50W-x8	Two-step Amberlite 743 and Biorad AG50W-x8 resin	IRA743 resin micro-sublimation	Single-stage AG50W-x12	AG50W-x12, P507 resin for Sr and Nd AG1W-x8, (100-200 mesh) for Pb	AG50W-x12 for Mg Ln Spec resin for Nd and Hf Sr Spec resin for Sr and Pb	AG50W-x12 for Mg Richrom DGA resin for Nd and Hf Sr-specific resin for Sr and Pb
Whole procedure blank	< 5 ng for Li, < 20 ng for B	~ 18 pg	~ 610 pg	25–35 ng	~ 25 ng	~ 21 ng	250 pg Sr, 100 pg for Nd, and Pb 200pg for Pb	10 ng for Mg, 100 pg Sr, 50 pg for Nd, 50 pg for Hf and Pb 150 pg for Pb	10 ng for Mg, 100 pg Sr, 50 pg for Nd, 50 pg for Hf and Pb 150 pg for Pb
Data reduction	SSB method for Li using NIST SRM 8485	SSB method for Li using L-SVEC	SSB method for Li using	SSB method for B using	SSB method for B using NBS 951	SSB method for Si using	Exponential law Sr ($^{86}Sr/^{88}Sr=0.1194$),	Exponential law Sr ($^{86}Sr/^{88}Sr=0.1194$),	Exponential law Sr ($^{86}Sr/^{88}Sr=0.1194$),

	SSB method for B using NBS 951		L-SVEC	NBS 951		NBS-28	Nd ($^{146}Nd/^{144}Nd$=0.7219) SSB method for Pb using NIST SRM 981	Nd ($^{146}Nd/^{144}Nd$=0.7219) Hf ($^{179}Hf/^{177}Hf$=0.7325) Pb (Tl doping using NIST SRM 997)	Nd ($^{146}Nd/^{144}Nd$=0.7219) Hf ($^{179}Hf/^{177}Hf$=0.7325) Pb (Tl doping using NIST SRM 997)
Standard solutions	-	L-SVEC: 0.03±0.20 (2*s*, *n* = 20) GSB-Li: 5.35 ± 0.17 (2*s*, *n* = 6) IRMM-016: 0.10 ± 0.25 (2*s*, *n* = 5)	L-SVEC: 0.00±0.22 (2*s*, *n* = 11)	NBS 951: -0.42±0.56 (2*s*, *n* = 15) IAEA RM B1: 39.38±0.27 (2*s*, *n* = 7) IAEA RM B-5: -4.30±0.36 (2*s*, *n* = 2)	AE121: 19.56±0.20 (2*s*, *n* = 1)[1] 19.60±0.16 (2*s*, *n* = 1)[2] AE122: 39.30±0.43 (2*s*, *n* =1)[1] 39.50±0.32 (2*s*, *n* =1)[2] SPEX-B:	USTC-Si: -0.07±0.06 (2*s*, *n* =15)	NIST SRM 987: $^{87}Sr/^{86}Sr$ = 0.710255 ± 21 (2*s*, n = 6) JNdi-1: $^{143}Nd/^{144}Nd$ =0.512112 ± 11 (2*s*, *n* = 6) NIST SRM 981: $^{208}Pb/^{204}Pb$ = 36.682 ± 0.011 (2*s*, *n* =5), $^{207}Pb/^{204}Pb$= 15.484	Cambridge 1: $\delta^{26}Mg$ = -2.60 ± 0.05‰ (2*s*, *n* = 41) IGGMg1: $\delta^{26}Mg$ = -1.75 ± 0.04‰ (2*s*, *n* = 65) NIST SRM 987: $^{87}Sr/^{86}Sr$ = 0.710248 ± 12 (2*s*, *n* = 15) JNdi-1:	NIST SRM 987: $^{87}Sr/^{86}Sr$ = 0.710253 ± 12 (2*s*, *n* = 7) JNdi-1: $^{143}Nd/^{144}Nd$ =0.512110 ± 12 (2*s*, *n* = 7) JMC 475: $^{176}Hf/^{177}Hf$ = 0.282172 ± 18 (2*s*, *n* = 7)

In-house BN boric acid RM: 13.33±0.40 (2*s*, *n* = 3)	-0.49±0.17 (2*s*, *n* = 1)[2]	± 0.003 (2*s*, *n* =5) $^{206}Pb/^{204}Pb$ = 16.934 ± 0.003 (2*s*, *n* = 5)	$^{143}Nd/^{144}Nd$ =0.512115 ± 12 (2*s*, *n* = 15) Alfa Hf:: $^{176}Hf/^{177}Hf$ = 0.282189 ± 10 (2*s*, *n* = 15) NIST SRM 981: $^{208}Pb/^{204}Pb$ = 36.7018 ± 0.0085 (2*s*, *n* = 7), $^{207}Pb/^{204}Pb$ = 15.4826 ± 0.0025 (2*s*, *n* = 7) $^{206}Pb/^{204}Pb$ = 16.9298 ± 0.0036 (2*s*, *n* = 7)	NIST SRM 981: $^{208}Pb/^{204}Pb$ = 36.7219 ± 0.0090 (2*s*, *n* = 7), $^{207}Pb/^{204}Pb$= 15.4963 ± 0.0028 (2*s*, *n* = 7) $^{206}Pb/^{204}Pb$ = 16.9405 ± 0.0034 (2*s*, *n* = 7)

Quanlity control materials	JG2: δ^7Li: 0.036±0.06 (2*s*, *n* = 19) JR2: δ^7Li: 3.95±0.04 (2*s*, *n* = 18) ZIPE-TS: δ^{11}B: -13.86±0.07 (2*s*, *n* = 43) ZIPE-TB: δ^{11}B:-11.28±0.06 (2*s*, *n* = 43)	BCR-2: 2.76±0.37 (2*s*, *n* = 1) JCp-1: 16.85 ± 0.60 (2*s*, *n* = 1) GSR-12: 14.28 ± 0.55 (2*s*, *n* = 1)	-	JB2: 7.25±0.57 (2*s*, *n* = 3)	AGV2: -4.50±0.39 (2*s*, *n* = 1)[2] NASS-6: 39.41±0.22 (2*s*, *n* = 1)[2]	AGV-2: -0.20±0.06 (2*s*, *n* =27) BHVO-2: -0.27±0.06 (2*s*, *n* =18) BCR-2: -0.25±0.06 (2*s*, *n* =27)	BCR-2: ^{87}Sr/^{86}Sr = 0.705019 ± 12 (2*s*, *n* =3) ^{143}Nd/^{144}Nd =0.512619 ± 10 (2*s*, *n* =3) ^{208}Pb/^{204}Pb = 38.701 ± 0.017 (2SE, *n* =1), ^{207}Pb/^{204}Pb= 15.619 ± 0.016 (2SE, *n* = 1) ^{206}Pb/^{204}Pb = 18.745 ± 0.015 (2SE, *n* = 1)	BCR-2: δ^{26}Mg = -0.19 ± 0.05‰ (2*s*, *n* = 3) ^{87}Sr/^{86}Sr = 0.704998 ± 12 (2*s*, *n* = 3) ^{143}Nd/^{144}Nd =0.512640 ± 10 (2*s*, *n* = 3) ^{176}Hf/^{177}Nd =0.282866 ± 6 (2*s*, *n* = 3) BHVO-2: δ^{26}Mg = -0.21 ± 0.04‰ GSP-2: δ^{26}Mg = -0.02 ± 0.03‰ GSR-3: ^{87}Sr/^{86}Sr = 0.704090	BCR: ^{87}Sr/^{86}Sr = 0.705032 ± 11 (2*s*, *n* = 3) ^{143}Nd/^{144}Nd =0.512649 ± 14 (2*s*, *n* = 3) ^{176}Hf/^{177}Hf =0.282862 ± 6 (2*s*, *n* = 3) AGV-2: ^{87}Sr/86Sr = 0.703981 ± 10 (2*s*, *n* = 3) ^{143}Nd/^{144}Nd =0.512801 ± 17 (2*s*, *n* = 3) ^{176}Hf/^{177}Nd =0.282970 ± 3 (2*s*, *n* = 3)

	± 16 (2*s*, *n* = 3)
	$^{143}Nd/^{144}Nd$ =0.512900 ± 12 (2*s*, *n* = 3)
	$^{176}Hf/^{177}Nd$ =0.282990 ± 6 (2*s*, *n* = 3)

Table 3.

New EPMA major element data for ARM-1, -2 and -3 glasses from three instruments

	ICP-OES*	**ICP-OES***	**XRF***	**EPMA***	**LA-ICP-MS***	**EPMA[1a]**	**EPMA[1b]**	**EPMA[2a]**	**EPMA[1b]**
	***n* = 4**	***n* = 4**	***n* = 3**	***n* = 30**	***n* = 225**	***n* = 50**	***n* = 50**	***n* = 30**	***n* = 50**
ARM-1									
SiO_2	-	58.4	58.1	58.7	-	58.72	58.61	59.09	59.06
TiO_2	0.94	1.02	0.99	0.99	0.95	1.00	0.99	0.98	1.01
Al_2O_3	13.2	13.3	13.4	13.4	-	13.41	13.37	13.04	13.50
FeO(t)	5.67	5.79	5.61	5.79	-	5.76	5.74	5.56	5.83
MnO	0.05	0.05	~~0.02~~	0.04	0.05	0.04	0.04	0.05	0.04
MgO	3.64	3.95	3.75	3.76	-	3.62	3.60	3.64	3.79
CaO	5	5.09	5.08	5.12	-	5.08	5.08	5.04	5.20
Na_2O	4.47	4.44	4.43	4.36	-	4.45	4.44	4.35	~~4.15~~
K_2O	3.11	3.16	3.13	3.12	-	3.19	3.17	3.13	3.23
P_2O_5	-	0.25	0.27	0.26	0.27	0.27	0.27	0.28	0.24
ARM-2									
SiO_2	-	58.3	57.6	57.8	-	58.06	57.86	58.16	58.35
TiO_2	0.92	1.03	0.97	0.97	0.99	0.98	0.97	0.97	1.00

Al_2O_3	13	13.3	13	13.1	-	13.20	13.18	12.90	13.24
FeO(t)	5.63	5.84	5.68	5.71	-	5.66	5.66	5.47	5.73
MnO	0.05	0.05	0.05	0.06	0.06	0.05	0.05	0.06	0.05
MgO	3.65	3.9	3.76	3.65	-	3.60	3.60	3.61	3.75
CaO	4.89	5.04	5.06	5.05	-	4.96	4.96	4.93	5.10
Na_2O	4.36	4.44	4.48	4.4	-	4.44	4.43	4.38	4.35
K_2O	2.92	3.04	3	3.05	-	3.00	3.00	2.90	3.02
P_2O_5	-	0.3	0.28	0.3	0.28	0.27	0.26	0.26	0.24
ARM-3									
SiO_2	-	60.8	60.3	60.4	-	60.61	60.56	61.07	60.85
TiO_2	0.97	1.06	1.01	1.02	1.01	1.03	1.03	1.02	1.05
Al_2O_3	13.8	13.8	13.8	13.8	-	13.96	13.96	13.70	14.01
FeO(t)	5.95	5.77	5.92	6	-	5.98	5.97	5.82	6.01
MnO	0.05	0.05	0.05	0.05	0.05	0.05	0.05	0.05	0.05
MgO	3.41	3.63	3.52	3.5	-	3.39	3.40	3.46	3.54
CaO	5.25	5.34	5.37	5.34	-	5.29	5.30	5.29	5.45
Na_2O	4.64	4.62	4.64	4.74	-	4.73	4.74	4.72	4.53
K_2O	3.14	3.25	3.16	3.18	-	3.20	3.18	3.14	3.25
P_2O_5	-	0.26	0.28	0.31	0.28	0.29	0.27	0.33	0.25

Data annotated with the superscript "*" were taken from a previous study (Wu *et al*. 2019). Data annotated with the superscripts "1a" and "1b" were obtained in two sessions using a JEOL JXA 8900Rl instrument at the GZG. Data annotated with the superscripts "2a" and "2b" were obtained using a JEOL JXA 8100 and a CAMECA SX Five, respectively, at IGGCAS. Data marked with a horizontal line were identified as outliers by the Dixon and Grubbs tests.

Table 4.

δ^7Li and δ^{11}B values for ARM-1, -2 and -3 glasses. Five laboratories reported bulk MC-ICP-MS data. δ^7Li and δ^{11}B values obtained from LA-MC-ICP-MS and SIMS are also listed

ARM glass	Institute	Technique	δ^7Li	Error (2*s*)	δ^{11}B	Error (2□)
ARM-1						
Split 1	CUG	MC-ICP-MS	0.47	0.24	-	-
Split 2		MC-ICP-MS	-	-	-	-
Split 3		MC-ICP-MS	0.69	0.29	-	-
Split 4	BRIUG	MC-ICP-MS	0.74	0.41	-	-
Split 5	GFZ	MC-ICP-MS	0.29	0.16	-12.06	0.34
Split 6		MC-ICP-MS	0.34	0.19	-11.68	0.36
Split 7		MC-ICP-MS	0.37	0.24	-11.76	0.27
Split 8		MC-ICP-MS	0.48	0.15	-11.91	0.17
Split 9		MC-ICP-MS	0.46	0.23	-11.80	0.16
Split 10		MC-ICP-MS	0.28	0.16	-11.74	0.04
Split 11	IGG-CNR	MC-ICP-MS	-	-	-	-
Split 12-22	IGGCAS	LA-MC-ICP-MS	0.90	0.69	-	-
Split 12-22	GIGCAS	LA-MC-ICP-MS	-	-	-11.82	0.57

	Split 23	UE	SIMS	-	-	-13.5	0.60
ARM-2							
	Split 1		MC-ICP-MS	0.68	0.31	-	-
	Split 2	CUG	MC-ICP-MS	0.31	0.07	-	-
	Split 3		MC-ICP-MS	0.36	0.05	-	-
	Split 4	BRIUG	MC-ICP-MS	0.95	0.32	-	-
	Split 5		MC-ICP-MS	0.52	0.14	-12.61	0.29
	Split 6		MC-ICP-MS	0.44	0.12	-12.54	0.14
	Split 7	GFZ	MC-ICP-MS	0.39	0.24	-12.50	0.15
	Split 8		MC-ICP-MS	0.58	0.17	-12.38	0.20
	Split 9		MC-ICP-MS	0.39	0.11	-12.66	0.18
	Split 10		MC-ICP-MS	0.45	0.19	-12.57	0.09
	Split 11	IGG-CNR	MC-ICP-MS	-	-	-12.75	0.05
	Split 12		MC-ICP-MS[1]	-	-	-12.74	0.09
	Split 13	IEECAS	MC-ICP-MS[1]	-	-	-12.87	0.59
	Split 14		MC-ICP-MS[2]	-	-	-12.86	0.33
	Split 15		MC-ICP-MS[2]	-	-	-12.43	0.38
	Split 16-26	IGGCAS	LA-MC-ICP-MS	6.08	0.54	-	-
	Split 16-26	GIGCAS	LA-MC-ICP-MS	-	-	-12.46	0.60

ARM-3						
Split 1		MC-ICP-MS	3.88	0.41	-	-
Split 2	CUG	MC-ICP-MS	3.83	0.12	-	-
Split 3		MC-ICP-MS	-	-	-	-
Split 4	BRIUG	MC-ICP-MS	3.80	0.19	-	-
Split 5		MC-ICP-MS	2.85	0.16	-3.24	0.18
Split 6		MC-ICP-MS	2.55	0.15	-3.04	0.22
Split 7		MC-ICP-MS	3.20	0.10	-2.57	0.27
Split 8	GFZ	MC-ICP-MS	3.79	0.24	-6.77	0.25
Split 9		MC-ICP-MS	3.30	0.22	-5.66	0.18
Split 10		MC-ICP-MS	3.14	0.14	-3.25	0.26
Split 11		MC-ICP-MS	-	-	-2.72	0.39
Split 12		MC-ICP-MS	-	-	-2.45	0.18
Split 13	IGG-CNR	MC-ICP-MS	-	-	-3.76	0.03
Split 14-24	IGGCAS	LA-MC-ICP-MS	4.10	2.89	-	-
Split 14-24	GIGCAS	LA-MC-ICP-MS	-	-	-3.40	1.19
Split 25	UE	SIMS	-	-	-3.80	0.40

The mean and 2 standard deviation (2*s*) values were calculated from the bulk MC-ICP-MS data. Instrument annotated with the superscripts “1”

and “2” refer to the purification technique “ion exchange chromatography” and “micro-sublimation”, respectively.

Table 5.

$\delta^{17}O$, $\delta^{18}O$, and $\Delta'^{17}O_{0.528}$ values for ARM-1, -2 and -3 glasses. $\delta^{18}O$ values obtained by SIMS are also listed

ARM glass		Institute	Technique	$\delta^{18}O$ [‰]	$\delta^{17}O$ [‰]	$\Delta^{17}O_{0.5305}$[ppm]
ARM-1						
	Split 1	GZG	Laser fluorination	5.71	2.95	-63
	Split 2			5.59	2.92	-
	Split 3	IGGCAS	nickel vessel fluorination	5.86	-	-
	Split 4			6.10	-	-
	Split 5			6.15	-	-
	Split 6			5.99	-	-
	Split 7	USTC	Laser fluorination	5.74	-	-
	Split 8			6.05	-	-
	Split 9			6.02	-	-
	Split 10-20	IGGCAS	SIMS	5.75	0.25	
ARM-2						
	Split 1	GZG	Laser fluorination	7.47	3.87	-73
	Split 2			7.45	3.86	-71
	Split 3	IGGCAS	nickel vessel	7.46	-	-

	Split 4		fluorination	7.48	-	-
	Split 5			7.44	-	-
	Split 6			7.01	-	-
	Split 7	USTC	Laser fluorination	7.00	-	-
	Split 8			7.12	-	-
	Split 9			7.16	-	-
	Split 10-20	IGGCAS	SIMS	5.95	0.21	-
ARM-3						
	Split 1	GZG	Laser fluorination	5.88	3.03	-65
	Split 2			5.68	2.92	-73
	Split 3	IGGCAS	nickel vessel fluorination	5.79	-	-
	Split 4			5.90	-	-
	Split 5			5.78	-	-
	Split 6-16	IGGCAS	SIMS	5.53	0.18	-

GZG data are normalised to the composition of San Carlos olivine with $\delta^{18}O = 5.17$ ‰ and $\Delta'^{17}O = -52$ ppm. Estimated measurement precisions (1*s*) are ±0.1 ‰ and ±11 ppm for $\delta^{18}O$ and $\Delta'^{17}O$ values from GZG, respectively. $\Delta'^{17}O = 1000[\ln(\delta^{17}O/1000+1) + 0.528 \times (1000\ln(\delta^{18}O/1000+1)]$.

Table 6.

$\delta^{29}Si$ and $\delta^{30}Si$ values (relative to NBS-28) for ARM-1, -2 and -3 glasses. Only one laboratory reported the $\delta^{29}Si$ and $\delta^{30}Si$ values. Two independent measurements yielded consistent results within measurement precision

ARM glass		**$\delta^{29}Si$**	**2*s***	**$\delta^{30}Si$**	**2*s***
ARM-1	Split 1	0.02	0.04	0.06	0.04
	Split 2	0.06	0.03	0.09	0.04
ARM-2	Split 1	0.03	0.03	0.05	0.01
	Split 2	0.04	0.03	0.03	0.03
ARM-3	Split 1	0.03	0.02	0.06	0.03

Table 7.

δ^{25}Mg and δ^{26}Mg values (relative to DSM3) of the three ARM glasses. Two laboratories reported the δ^{25}Mg and δ^{26}Mg values. A total of five independent measurements yielded consistent results within measurement precision

ARM glass		**Institute**	**Technique**	**δ^{25}Mg**	**2*s***	**δ^{26}Mg**	**2*s***
ARM-1	Split 1	IGGCAS	MC-ICP-MS	-0.58	0.03	-1.13	0.03
	Split 2		MC-ICP-MS	-0.57	0.02	-1.11	0.01
	Split 3		MC-ICP-MS	-0.56	0.03	-1.15	0.07
	Split 4	NWU	MC-ICP-MS	-0.55	0.02	-1.11	0.02
	Split 5		MC-ICP-MS	-0.56	0.05	-1.11	0.06
ARM-2	Split 1	IGGCAS	MC-ICP-MS	-0.57	0.03	-1.10	0.04
	Split 2		MC-ICP-MS	-0.57	0.04	-1.12	0.03
	Split 3		MC-ICP-MS	-0.53	0.04	-1.07	0.02
	Split 4	NWU	MC-ICP-MS	-0.53	0.02	-1.06	0.04
	Split 5		MC-ICP-MS	-0.52	0.03	-1.05	0.03
ARM-3	Split 1	IGGCAS	MC-ICP-MS	-0.61	0.03	-1.19	0.05
	Split 2		MC-ICP-MS	-0.61	0.03	-1.16	0.02
	Split 3		MC-ICP-MS	-0.56	0.02	-1.13	0.02
	Split 4	NWU	MC-ICP-MS	-0.57	0.03	-1.14	0.07

Table 8.

TIMS and MC-ICP-MS $^{87}Sr/^{86}Sr$, $^{143}Nd/^{144}Nd$ and $^{176}Hf/^{177}Hf$ ratio data for the three ARM glasses

ARM glass	Method	$^{87}Sr/^{86}Sr$	Error (2*s*)	$^{143}Nd/^{144}Nd$	Error (2*s*)	$^{176}Hf/^{177}Hf$	Error (2*s*)
ARM-1							
Split 1	TIMS[1]	0.707775	0.000011	0.512167	0.000006	-	-
Split 2	TIMS[1]	0.707770	0.000010	0.512174	0.000008	-	-
Split 3	TIMS[1]	0.707779	0.000010	0.512160	0.000006	-	-
Split 4	TIMS[1]	0.707752	0.000013	0.512163	0.000007	-	-
Split 5	TIMS[1]	0.707752	0.000010	0.512163	0.000006	-	-
Split 6	TIMS[1]	-	-	0.512168	0.000006	-	-
Split 7	TIMS[1]	-	-	0.512161	0.000006	-	-
Split 8	MC-ICP-MS[1]	0.707805	0.000013	0.512158	0.000009	0.282122	0.000003
Split 9	MC-ICP-MS[1]	0.707783	0.000017	0.512148	0.000008	0.282128	0.000003
Split 10	MC-ICP-MS[1]	0.707784	0.000014	0.512159	0.000006	0.282126	0.000002
Split 11	MC-ICP-MS[2]	0.707806	0.000013	0.512171	0.000009	0.282128	0.000003
Split 12	MC-ICP-MS[2]	0.707805	0.000017	0.512169	0.000008	0.282127	0.000003
Split 13	MC-ICP-MS[2]	0.707805	0.000014	0.512169	0.000006	0.282120	0.000002
ARM-2							

Split 1	TIMS[1]	0.708028	0.000012	0.512130	0.000008	-	-
Split 2	TIMS[1]	0.708031	0.000013	0.512120	0.000008	-	-
Split 3	TIMS[1]	0.708019	0.000012	0.512123	0.000007	-	-
Split 4	TIMS[1]	0.708035	0.000010	0.512119	0.000008	-	-
Split 5	TIMS[1]	0.708010	0.000009	0.512134	0.000007	-	-
Split 6	TIMS[1]	0.708008	0.000013	0.512132	0.000007	-	-
Split 7	TIMS[1]	0.708018	0.000014	0.512134	0.000008	-	-
Split 8	MC-ICP-MS[1]	0.708031	0.000015	0.512121	0.000009	0.282134	0.000003
Split 9	MC-ICP-MS[1]	0.708028	0.000014	0.512127	0.000010	0.282127	0.000003
Split 10	MC-ICP-MS[1]	0.708034	0.000010	0.512115	0.000010	0.282120	0.000003
Split 11	MC-ICP-MS[2]	-	-	0.512134	0.000009	0.282126	0.000003
Split 12	MC-ICP-MS[2]	-	-	0.512133	0.000010	0.282123	0.000003
Split 13	MC-ICP-MS[2]	-	-	0.512134	0.000010	0.282118	0.000003
ARM-3							
Split 1	TIMS[1]	-	-	0.512082	0.000009	-	-
Split 2	TIMS[1]	0.708808	0.000009	0.512096	0.000008	-	-
Split 3	TIMS[1]	0.708799	0.000008	0.512084	0.000008	-	-
Split 4	TIMS[1]	0.708797	0.000015	0.512083	0.000008	-	-
Split 5	TIMS[1]	0.708822	0.000012	0.512090	0.000007	-	-

Split 6	TIMS[1]	0.708838	0.000010	0.512106	0.000008	-	-
Split 7	TIMS[1]	0.708796	0.000008	0.512088	0.000009	-	-
Split 8	MC-ICP-MS[1]	0.708784	0.000017	0.512076	0.000017	-	-
Split 9	MC-ICP-MS[1]	0.708786	0.000013	0.512089	0.000017	-	-
Split 10	MC-ICP-MS[1]	0.708796	0.000014	0.512083	0.000009	-	-
Split 11	MC-ICP-MS[2]	0.708835	0.000017	-	-	0.282136	0.000003
Split 12	MC-ICP-MS[2]	0.708832	0.000013	-	-	0.282135	0.000002
Split 13	MC-ICP-MS[2]	0.708828	0.000014	-	-	0.282137	0.000003

The analytical errors are given as 2*s*. Instrument annotated with the superscripts “1” and “2” is from IGGCAS and NWU, respectively.

Table 9.

$^{206}Pb/^{204}Pb$, $^{207}Pb/^{204}Pb$, $^{208}Pb/^{204}Pb$, $^{207}Pb/^{206}Pb$ and $^{208}Pb/^{206}Pb$ ratios for ARM-1, -2 and -3 glasses. The mean values (n = 100) from LA-MC-ICP-MS analysis are also listed

ARM glass	Method	$^{208}Pb/^{204}Pb$	$^{207}Pb/^{204}Pb$	$^{206}Pb/^{204}Pb$	$^{208}Pb/^{206}Pb$	$^{207}Pb/^{206}Pb$
ARM-1						
Split 1	TIMS[1]	38.542	15.670	18.389	2.0960	0.85216
Split 2	TIMS[1]	38.543	15.670	18.388	2.0961	0.85216
Split 3	TIMS[1]	38.576	15.680	18.397	2.0968	0.85233
Split 4	MC-ICP-MS[2]	38.535	15.666	18.387	2.0957	0.85202
Split 5	MC-ICP-MS[2]	38.541	15.668	18.389	2.0959	0.85206
Split 6	MC-ICP-MS[2]	38.542	15.668	18.389	2.0960	0.85206
Split 7-32	LA-MC-ICP-MS	38.5000	15.672	18.399	2.0949	0.85219
ARM-2						
Split 1	MC-ICP-MS[1]	38.517	15.661	18.386	2.0949	0.85178
Split 2	MC-ICP-MS[1]	38.516	15.660	18.386	2.0949	0.85178
Split 3	MC-ICP-MS[2]	38.563	15.672	18.396	2.0963	0.85194
Split 4	MC-ICP-MS[2]	38.563	15.672	18.396	2.0963	0.85192
Split 5	MC-ICP-MS[2]	38.563	15.672	18.395	2.0964	0.85196
Split 6-31	LA-MC-ICP-MS	38.510	15.675	18.404	2.0954	0.85174
ARM-3						
Split 1	TIMS[1]	38.664	15.685	18.437	2.0970	0.85070
Split 2	TIMS[1]	38.691	15.692	18.443	2.0979	0.85083
Split 3	TIMS[1]	38.704	15.696	18.447	2.0981	0.85086
Split 4	MC-ICP-MS[2]	38.661	15.682	18.436	2.0971	0.85062
Split 5	MC-ICP-MS[2]	38.660	15.682	18.436	2.0970	0.85061
Split 6	MC-ICP-MS[2]	38.664	15.683	18.437	2.0972	0.85063
Split 7-32	LA-MC-ICP-MS	38.674	15.704	18.468	2.0966	0.85036

Instrument annotated with the superscripts "1" and "2" is from IGGCAS and NWU, respectively.

Table 10.

$Fe^{2+}/\Sigma Fe$ ratios for ARM-1, -2 and -3 glasses. The data were obtained from two laboratories (LUH and IGGCAS). Two laboratories reported the $\delta^{25}Mg$ and $\delta^{26}Mg$ values. A total of four independent measurements yielded consistent results within measurement precision

			ARM-1		**ARM-2**		**ARM-3**	
Laboratory	**date**	***n***	**$Fe^{2+}/\Sigma Fe$**	**2*s***	**$Fe^{2+}/\Sigma Fe$**	**2*s***	**$Fe^{2+}/\Sigma Fe$**	**2*s***
LUH	2019/2/7	3	0.29	0.02	0.30	0.02	0.30	0.02
LUH	2019/2/28	3	0.29	0.02	0.30	0.02	0.30	0.02
LUH	2019/3/7	3	0.29	0.02	0.30	0.02	0.29	0.02
IGGCAS	2020/6/28	3	0.32	0.03	0.30	0.03	0.31	0.03

Table 11.

New reference values for the major elements and the Li-B-Si-O-Mg-Sr-Nd-Hf-Pb isotopic ratios and $Fe^{2+}/\Sigma Fe$ ratios of the ARM-1, -2 and -3 glasses

	ARM-1					**ARM-2**					**ARM-3**				
	Value	***p***	**2*s***	**2SE**	**Cl**	**Value**	***p***	**2*s***	**2SE**	**Cl**	**Value**	***p***	**2*s***	**2SE**	**Cl**
SiO_2	58.67	7	0.70	0.26	0.32	58.02	7	0.55	0.21	0.26	60.66	7	0.54	0.20	0.25
TiO_2	0.99	9	0.05	0.02	0.02	0.98	9	0.06	0.02	0.02	1.02	9	0.05	0.02	0.02
Al_2O_3	13.33	8	0.29	0.10	0.12	13.11	8	0.28	0.10	0.12	13.85	8	0.22	0.08	0.09
FeO(t)	5.72	8	0.19	0.07	0.08	5.67	8	0.21	0.07	0.09	5.93	8	0.18	0.06	0.07
MnO	0.041	9	0.020	0.007	0.008	0.054	9	0.009	0.003	0.003	0.049	9	0.003	0.001	0.001
MgO	3.72	8	0.24	0.08	0.10	3.69	8	0.21	0.07	0.09	3.48	8	0.17	0.06	0.07
CaO	5.09	8	0.12	0.04	0.05	5.00	8	0.15	0.05	0.06	5.33	8	0.12	0.04	0.05
Na_2O	4.39	8	0.21	0.07	0.09	4.41	8	0.09	0.03	0.04	4.67	8	0.15	0.05	0.06
K_2O	3.15	8	0.08	0.03	0.03	2.99	8	0.11	0.04	0.04	3.19	8	0.09	0.03	0.04
P_2O_5	0.26	8	0.03	0.01	0.01	0.27	8	0.04	0.01	0.02	0.28	8	0.05	0.02	0.02
$Fe^{2+}/\Sigma Fe$	0.31	2	0.05	0.03	0.20	0.30	2	-	-	-	0.30	2	0.02	0.01	0.09
δ^7Li	0.56	3	0.37	0.22	0.46	0.62	3	0.58	0.33	0.72	3.60	3	0.80	0.46	0.99
$\delta^{11}B$	-11.82	1	-	-	-	-12.63	2	0.26	0.18	1.16	-3.68	2	0.08	0.06	0.38

$\delta^{17}O$	5.88	3	0.20	0.12	0.51	7.33	3	0.22	0.13	0.56	5.80	2	0.03	0.02	0.28
$\delta^{18}O$	2.93	1	-	-	-	3.86	1	-	-	-	2.98	1	-	-	-
$\Delta^{17}O_{0.5305}$	-63.10	1	-	-	-	-72.16	1	-	-	-	-69.17	1	-	-	-
$\delta^{29}Si$	0.04	1	-	-	-	0.03	1	-	-	-	0.03	1	-	-	-
$\delta^{30}Si$	0.08	1	-	-	-	0.04	1	-	-	-	0.05	1	-	-	-
$\delta^{25}Mg$	-0.56	2	0.02	0.02	0.11	-0.55	2	0.06	0.04	0.28	-0.59	2	0.07	0.05	0.29
$\delta^{26}Mg$	-1.12	2	0.01	0.01	0.04	-1.09	2	0.07	0.05	0.34	-1.16	2	0.06	0.04	0.28
$^{87}Sr/^{86}Sr$	0.707787	3	0.000040	0.000023	0.000050	0.708026	2	0.000014	0.000010	0.000062	0.708810	3	0.000043	0.000025	0.000054
$^{143}Nd/^{144}Nd$	0.512163	3	0.000015	0.000009	0.000019	0.512127	3	0.000013	0.000007	0.000016	0.512086	2	0.000010	0.000007	0.000045
$^{176}Hf/^{177}Hf$	0.282125	2	-	-	-	0.282125	2	0.000007	0.000005	0.000030	0.282136	1	-	-	-
$^{208}Pb/^{204}Pb$	38.546	2	0.020	0.014	0.089	38.548	2	0.044	0.031	0.198	38.674	2	0.035	0.025	0.156
$^{207}Pb/^{204}Pb$	15.671	2	0.008	0.006	0.035	15.668	2	0.011	0.008	0.048	15.686	2	0.012	0.009	0.055
$^{206}Pb/^{204}Pb$	18.390	2	0.004	0.003	0.019	18.392	2	0.009	0.006	0.041	18.439	2	0.009	0.006	0.041
$^{208}Pb/^{206}Pb$	2.0961	2	0.0006	0.0004	0.0027	2.0959	2	0.0014	0.0010	0.0062	2.0974	2	0.0008	0.0006	0.0038
$^{207}Pb/^{206}Pb$	0.85213	2	0.00024	0.00017	0.00107	0.85189	2	0.00016	0.00011	0.00070	0.85071	2	0.00025	0.00018	0.00112

The uncertainties for the reference values are given at the 95% confidence level. Also shown is the number *p* of values (*n*) contributing to the recommended values. The CI and 2SE are only meaningful with $p > 7$. For the isotope ratios and $Fe^{2+}/\Sigma Fe$ ratios, the reference values are calculated based on the data from the bulk measurement principles (TIMS, MC-ICP-MS, IR-MS, and wet-chemistry colorimetry). In the case of

p = 1, the 2*s*, 2SE and Cl could not be calculated and thus marked as "-". In several case of *p* = 1, two laboratories reported identical values, and the 2*s*, 2SE and Cl could not be calculated and thus also marked as "-".

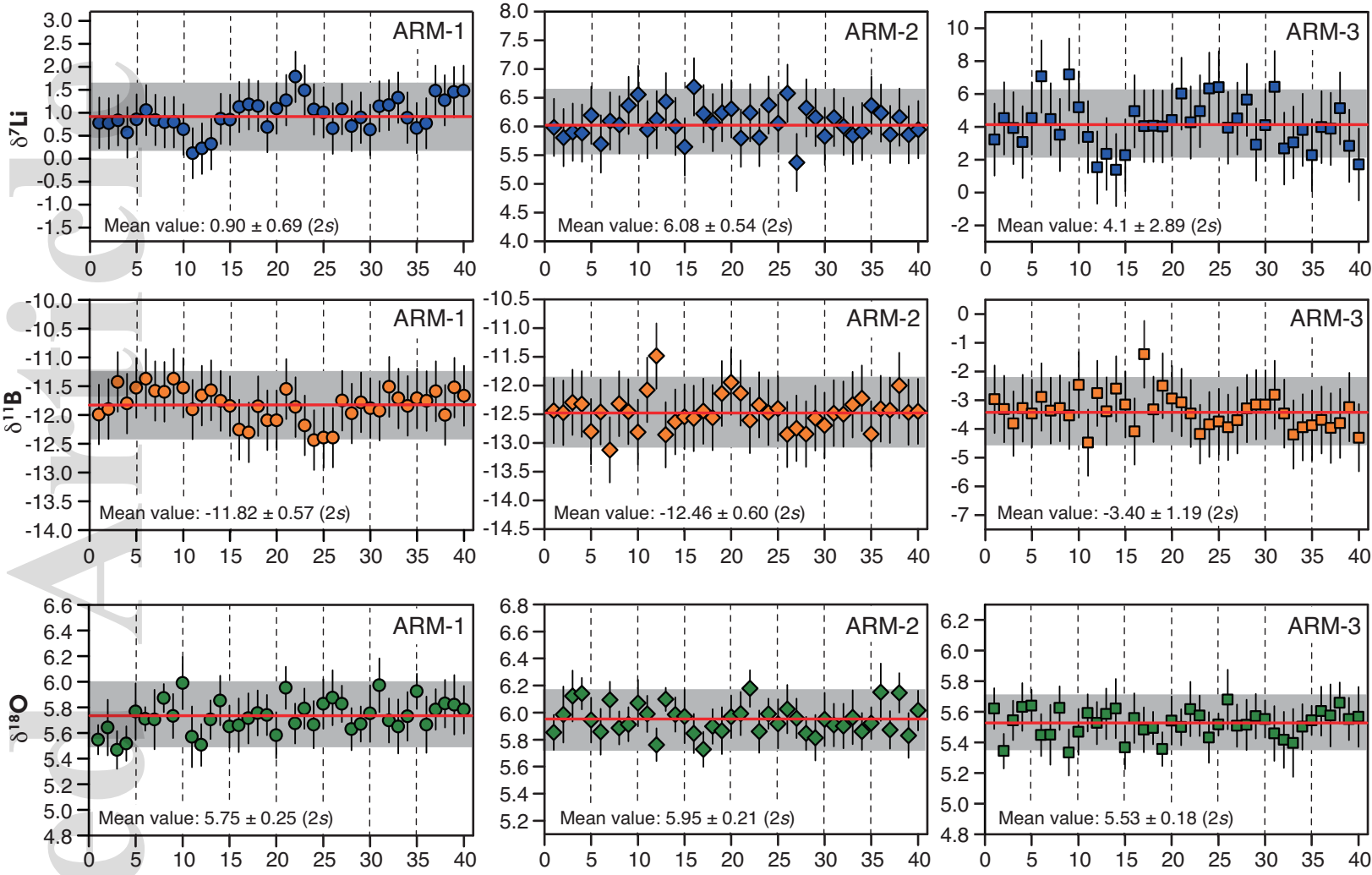

ggr_12399_f1.eps

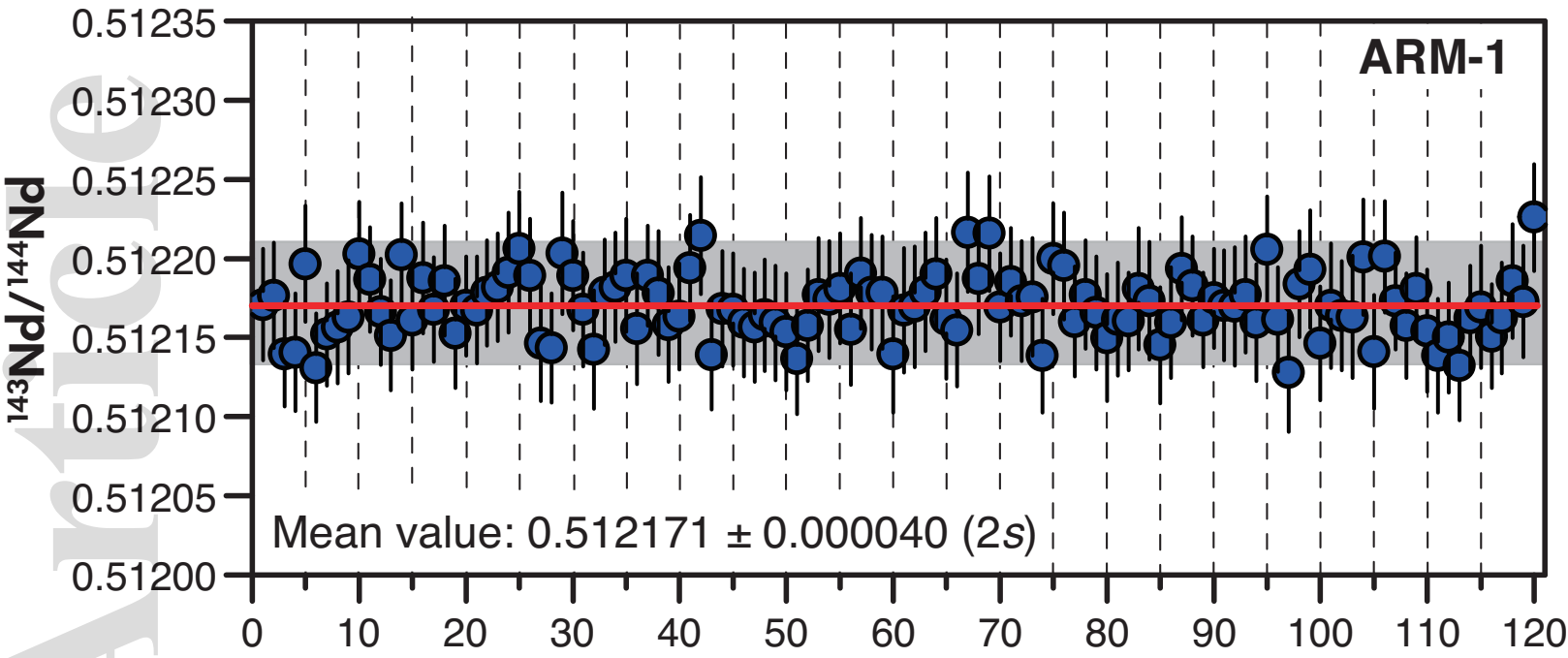

ggr_12399_f2.eps

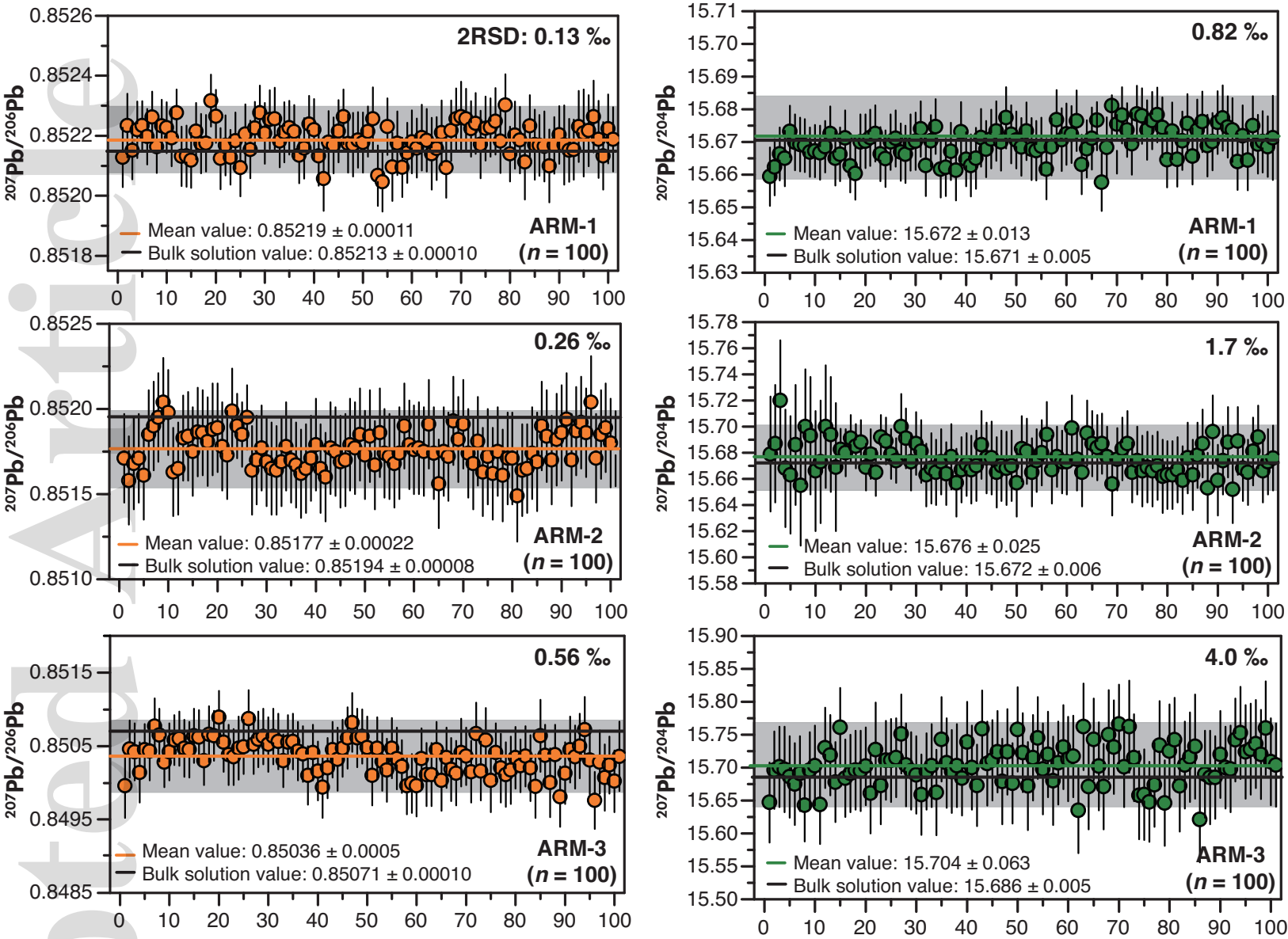

ggr_12399_f3.eps

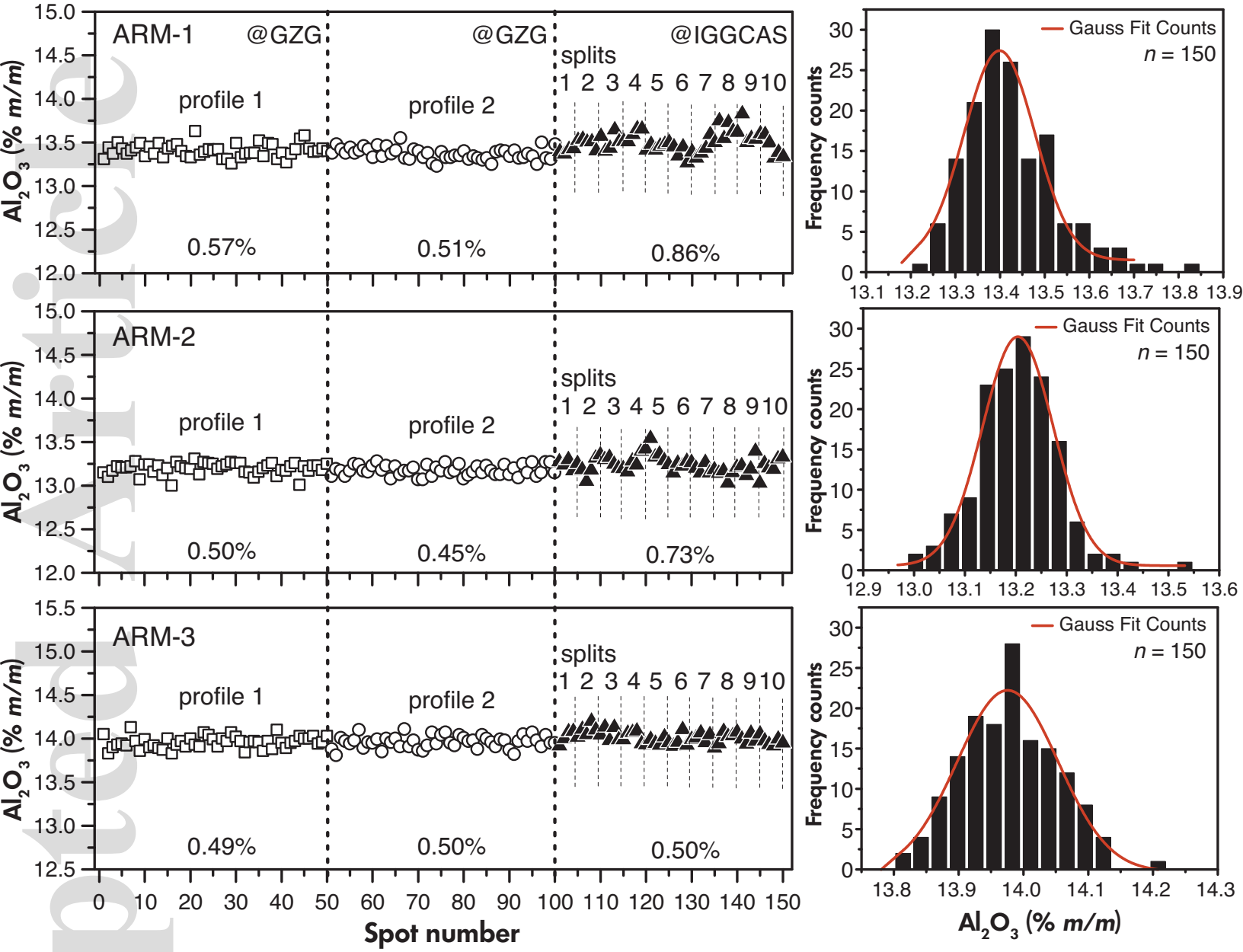

ggr_12399_f4.eps

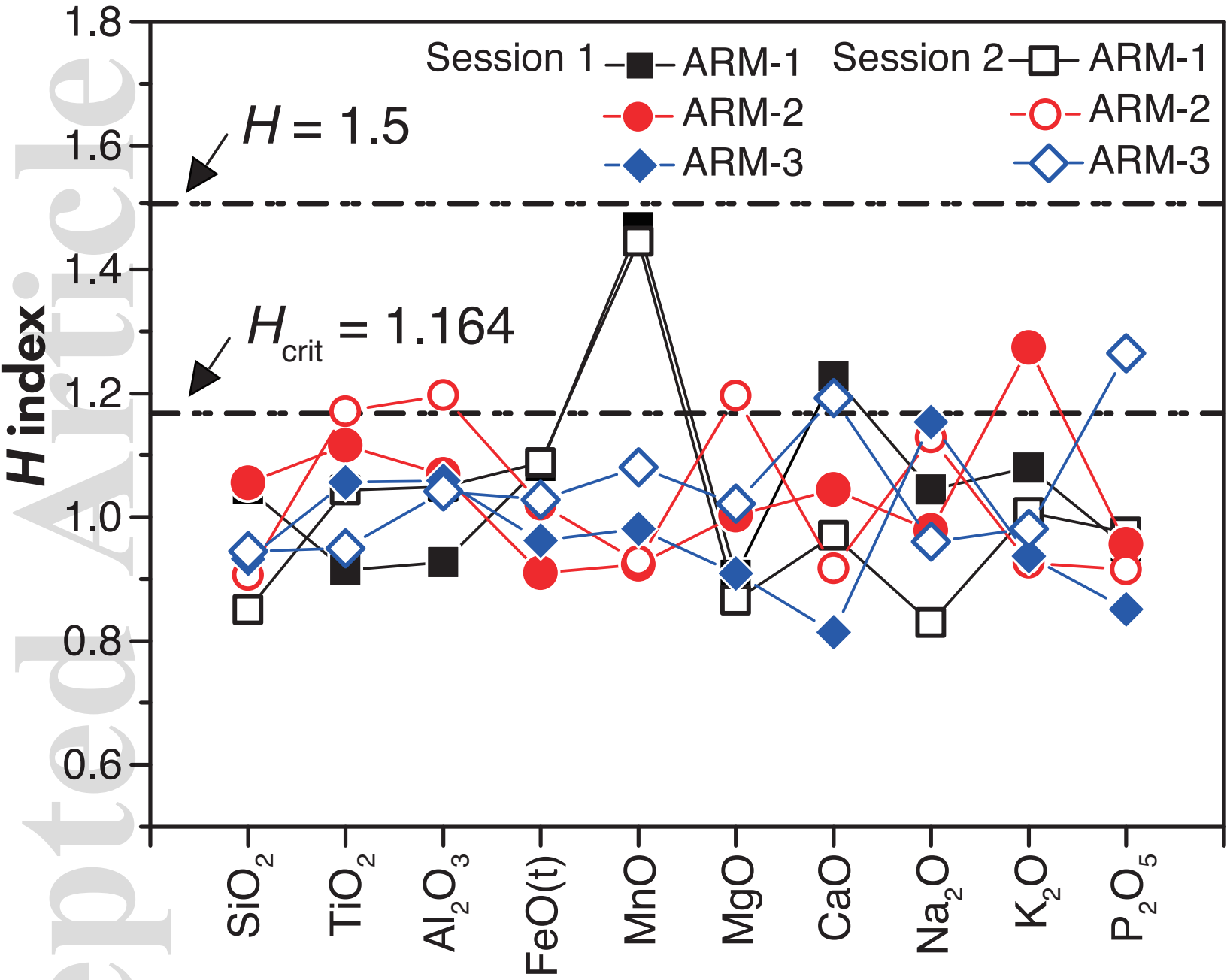

ggr_12399_f5.eps

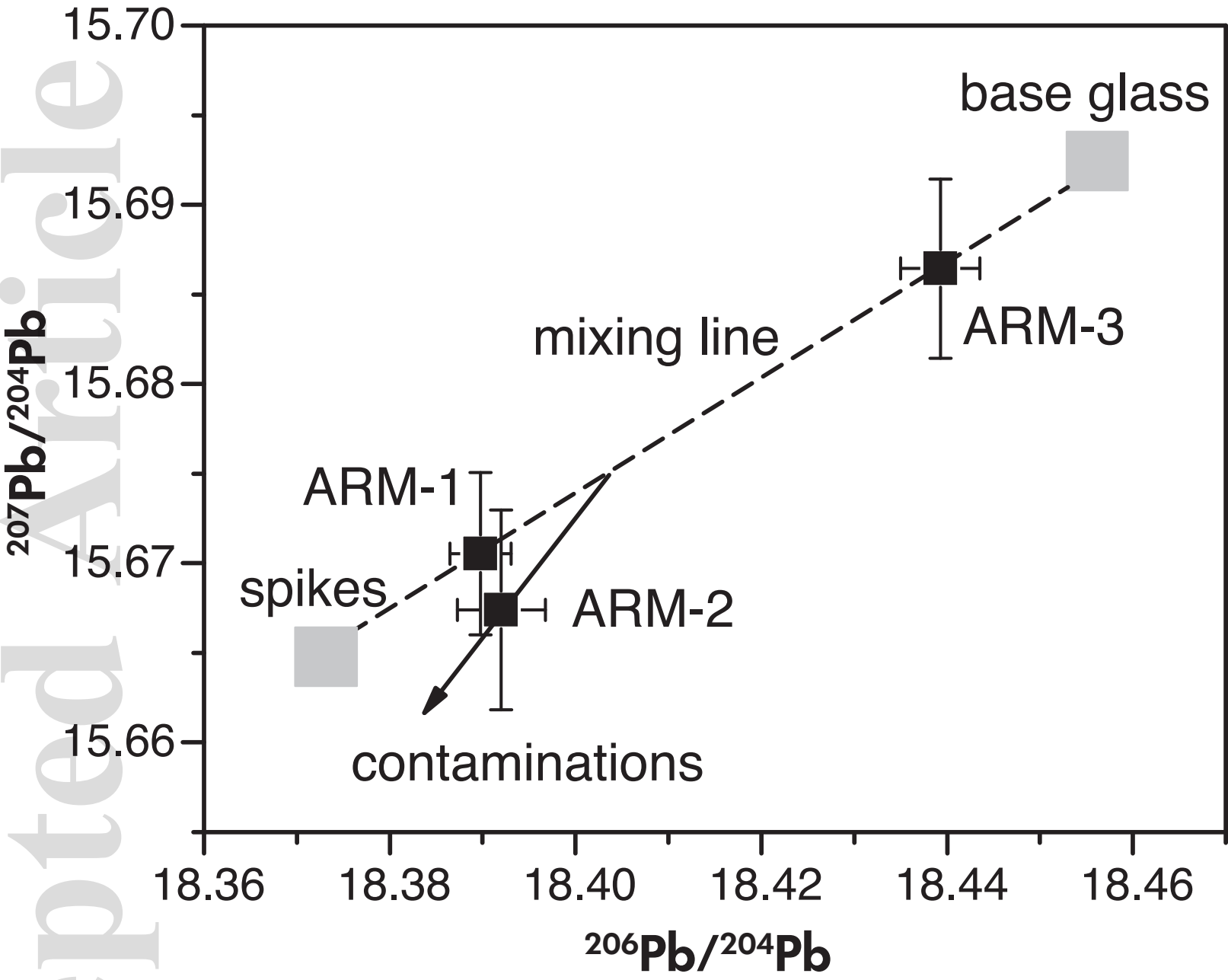

ggr_12399_f6.eps

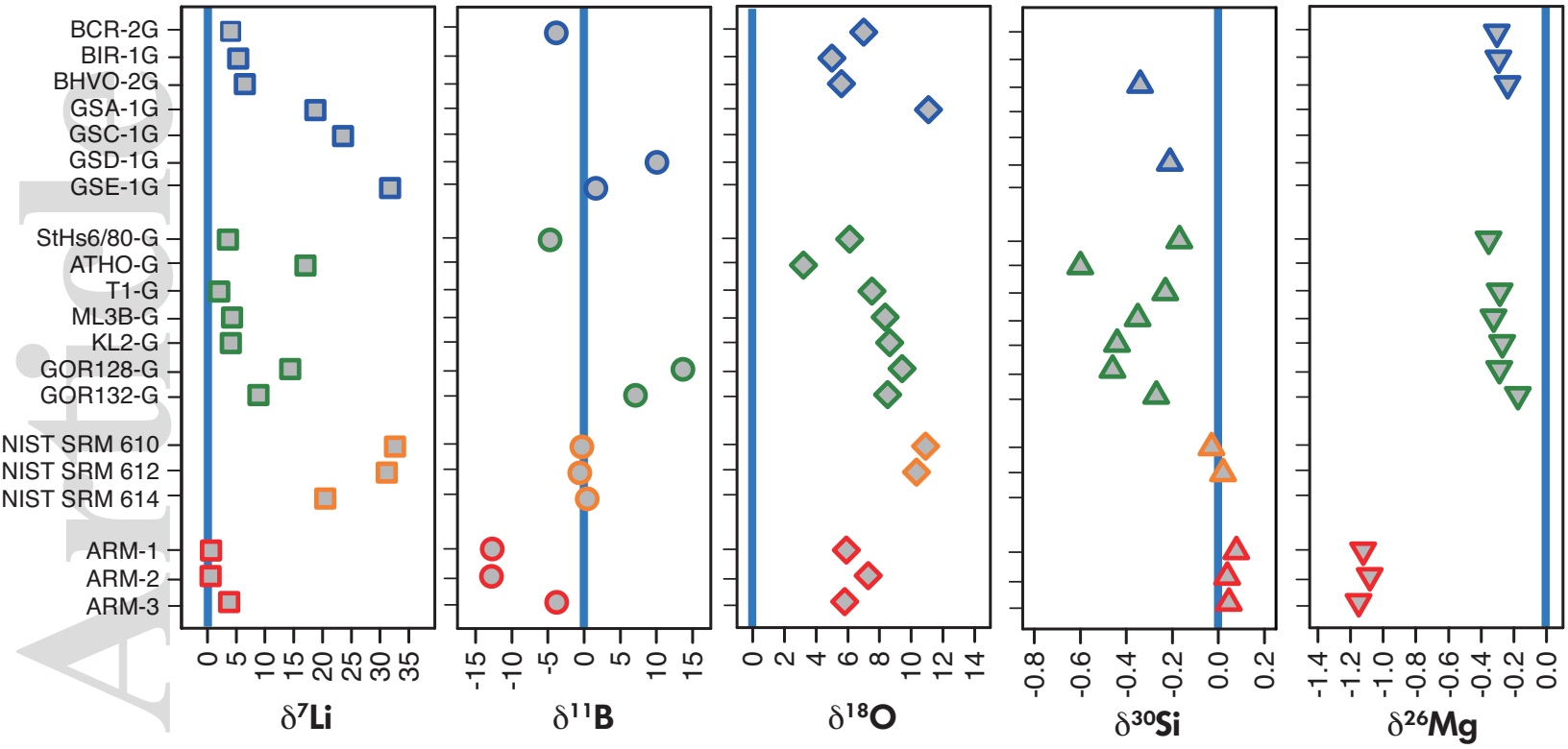

ggr_12399_f7.eps

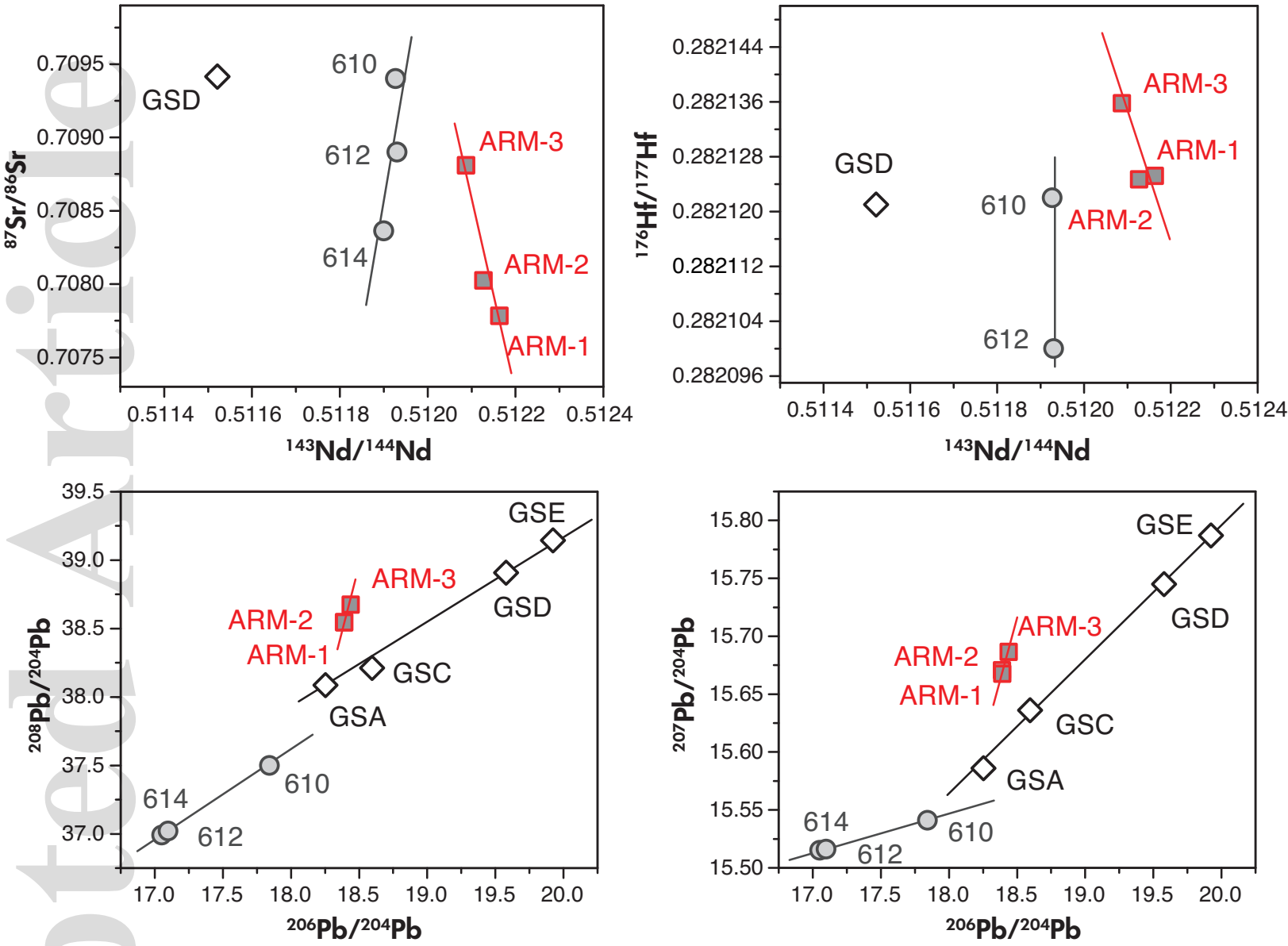

ggr_12399_f8.eps